System identification and prediction models in ship dynamics

From roll damping to manoeuvring

MARTIN ALEXANDERSSON

System identification and prediction models in ship dynamics
From roll damping to manoeuvring

MARTIN ALEXANDERSSON

System identification and prediction models in ship dynamics

MARTIN ALEXANDERSSON
Chalmers University of Technology
Department of Mechanics and Maritime Sciences

Abstract

This thesis investigates the enhancement of ship manoeuvring models through the integration of prior knowledge embedded in parametric model structures and semi-empirical formulas. The research is driven by the question: How can prior knowledge be used to enhance the generalization of ship manoeuvring models?

The study begins with a prestudy focusing on one degree of freedom in ship roll motion, aiming to develop parameter identification techniques and propose a parametric model structure with good generalization. This knowledge is then extended to the manoeuvring problem, with objectives including the development of parameter identification techniques for ship manoeuvring models, proposing a generalizable parametric model structure, mitigating multicollinearity, and identifying added masses.

Methodologically, the research employs various parametric model structures for roll motion and manoeuvring, investigated through free running model tests and virtual captive tests (VCT). A novel parameter identification method combining inverse dynamics with an extended Kalman filter (EKF) is proposed. Additionally, a deterministic semi-empirical rudder model is introduced to address multicollinearity issues.

Key findings indicate that inverse dynamics regression is an efficient method for parameter identification in parametric models. The proposed quadratic model structure for roll motion demonstrates good generalization, and the new parameter identification method identifies models that accurately predict standard maneuvers. However, challenges with multicollinearity and the need for more informative data are highlighted. The study concludes that semi-empirical formulas can guide identification towards more physically correct models, and VCT can provide the necessary data for accurate model identification.

The implications of this research suggest that integrating semi-empirical rudder models and utilizing VCT can enhance the accuracy and generalization of ship manoeuvring models, contributing to more reliable and physically accurate manoeuvring simulations.

Keywords: Manoeuvring, Roll damping, System identification, Extended Kalman filter, Inverse dynamics, Multicollinearity

Preface

This thesis presents research conducted since February 2020 in the Division of Marine Technology, Department of Mechanics and Marine Sciences at Chalmers University of Technology, and RISE (www.ri.se). Financial support for this research was provided by the DEMOPS project (Development of Methods for Operational Performance of Ships), funded by the Swedish Transport Administration (project: FP4 2020), and the D2E2F project (Data Driven Energy Efficiency of Ships), funded by the Swedish Energy Agency (project: 49301-1).

After several years of unsuccessful attempts to secure funding for my PhD studies, I was contacted by Professor Wengang Mao five years ago with an offer to become a PhD student. I am deeply grateful for this opportunity. Professor Mao has been my main supervisor throughout my studies, guiding me in academic research and teaching me about statistical and machine learning methods. My gratitude also extends to my examiner and co-supervisor, Professor Jonas W. Ringsberg, head of the Division of Marine Technology. I have greatly valued our discussions on research methodology and academic writing, and his meticulous proofreading has been a tremendous asset to our papers.

I would like to thank RISE and the head of the Research Department, Christian Finnsgård, for allowing me to pursue an industrial PhD. I am also grateful to my colleagues at RISE, including Martin Kjellberg, Olov Lundbäck, and others, for the insightful discussions we have had about ship dynamics, which have been invaluable to the literature study of this thesis. Finally, I want to acknowledge all the personnel at RISE who have been involved in model tests, building ship models, and conducting experiments.

Martin Alexandersson
Göteborg, March 2025

Contents

List of publications

This thesis is based on the following appended papers:

Paper 1   Alexandersson, M., Mao, W., and Ringsberg, J. W. (2021b). "Analysis of roll damping model scale data". In: *Ships and Offshore Structures*, vol 16 2021. DOI: 10.1080/17445302.2021.1907070.

Paper 2   Alexandersson, M., Kjellberg, M., Mao, W., and Ringsberg, J. W. (2021a). "Prediction of roll motion using fully nonlinear potential flow and Ikeda's method". In: *Proceedings of the Thirty-first (2021) International Ocean and Polar Engineering Conference*. Rhodes, Greece: International Society of Offshore and Polar Engineers (ISOPE).

Paper 3   Alexandersson, M., Mao, W., and Ringsberg, J. W. (2022a). "System identification of Vessel Manoeuvring Models". In: *Ocean Engineering* 266, p. 112940. DOI: 10.1016/j.oceaneng.2022.112940.

Paper 4   Alexandersson, M., Mao, W., Ringsberg, J. W., and Kjellberg, M. (2024). "System identification of a physics-informed ship model for better predictions in wind conditions". In: *Ocean Engineering* 310, p. 118613. issn: 0029-8018. DOI: 10.1016/ j.oceaneng.2024.118613.

Paper 5   Alexandersson, M., Mao, W., Ringsberg, J. W., and Kjellberg, M. (2025). "Identification of manoeuvring models for wind-assisted ships with large rudders using virtual captive tests". Manuscript submitted to: *International Journal of Naval Architecture and Ocean Engineering*.

Authors' contributions (CRediT):

Martin Alexandersson	Conceptualization, Methodology, Software, Validation, Formal analysis, Investigation, Resources, Writing - Original Draft, Writing - Review & Editing, Visualization (Paper 1–5).
Wengang Mao	Writing - Review & Editing, Supervision, Project administration, Funding acquisition (Paper 1–5).
Jonas W. Ringsberg	Writing - Review & Editing, Supervision (Paper 1–5).
Martin Kjellberg	Resources (Paper 2, 4, and 5)

Other publications co-authored by Martin Alexandersson:

Paper   Marimon Giovannetti, L., Olsson, F., Alexandersson, M., Werner, S., and Finnsgård, C. (2020). The Effects of Hydrodynamic Forces on Maneuvrability Coefficients for Wind-Assisted Ships. DOI: 10.1115/OMAE2020-18673.

Paper   Alexandersson, M., Zhang, D., Mao, W., and Ringsberg, J. W. (2022b). "A comparison of ship manoeuvrability models to approximate ship navigation trajectories". In: *Ships and Offshore Structures* https://DOI.org/10.1080/17445302.2022.2067409, pp. 1–8. issn: 1744-5302. DOI: 10.1080/17445302.2022.2067409.

Paper   Vergara, D., Alexandersson, M., Lang, X., and Wengang, M. (2023). "Power Allocation Influence on Energy Consumption of a Double-Ended Ferry". In: *ISOPE–I–23–551*.

Nomenclature

β	ship drift angle	rad
$\bigtriangledown$	ship displacement	m^3
δ	rudder angle	rad
υ	ship velocity vector	
$\mathbf{C}$	Coriolis-centripetal matrix	
$\mathbf{D}$	damping force vector	
$\mathbf{F}$	total force vector	
$\mathbf{M}$	system inertia matrix	
$\mathbf{x}$	ship state vector	
ω_0	natural angular velocity	rad/s
ϕ	ship roll angle	rad
ϕ_a	initial roll amplitude	rad
Ψ	ship heading	rad
ρ	water density	kg/m^3
$\mathbf{c}$	control signal	
$\mathbf{w}$	process noise	
A_0	mid ship area coefficient	-
A_{44}	total mass moment of inertia	kg·m^2
B_1	linear damping coefficient	Nm/(rad/s)
B_2	quadratic damping coefficient	Nm/(rad/s^2
B_3	cubic damping coefficient	Nm/(rad/s)^3
B_{BK}	bilge keel roll damping	Nm/(rad/s)
B_E	eddy roll damping	Nm/(rad/s)
B_F	friction roll damping	Nm/(rad/s)
B_L	hull lift roll damping	Nm/(rad/s)
B_W	wave roll damping	Nm/(rad/s)
$beam$	ship beam	m
BK_B	bilge keel height	m
BK_L	bilge keel length	m

C_1	linear stiffness coefficient	Nm/rad
C_3	stiffness coefficient	Nm/rad^3
C_5	stiffness coefficient	Nm/rad^5
D	propeller diameter	m
g	gravity	kg·m/s^2
GM	ship metacentric height	m
I_z	ship yaw moment of inertia	kg·m^2
J	propeller advance ratio	-
L	ship perpendicular length	m
m	ship mass	kg
N	ship yawing moment	Nm
n	propeller speed	rad/s
OG	vertical distance into water from still water to center of gravity	m
r	yaw rate	rad/s
T	mean draught	m
t	time	s
u	surge velocity	m/s
V	ship speed	m/s
v	sway velocity	m/s
w_p	propeller wake fraction	-
w_{p0}	Taylor wake fraction	-
X	ship force in longitudinal direction	N
x_0	ship global position	m
x_G	ship longitudinal center of gravity	m
x_p	propeller longitudinal position	m
Y	ship force in transverse direction	N
y_o	ship global position	m

List of acronyms

AVMM	–	Abkowitz vessel manoeuvring model
BB	–	black box
CFD	–	computational fluid dynamics
CMT	–	captive model test
CT	–	captive test
KF	–	Kalman filter
EKF	–	extended Kalman filter
FRMT	–	free running model tests
FFT	–	fast Fourier transform
FT	–	free-running test
GB	–	grey box
HSVA	–	Hamburg ship model basin
ID	–	inverse dynamics
IMO	–	International Maritime Organization
KVLCC2	–	Korean very large crude carrier 2nd generation
LVMM	–	linear vessel manoeuvring model
MARIN	–	maritime research institute Netherlands
MAVMM	–	modified Abkowitz vessel manoeuvring model
ML	–	machine learning
MMG	–	manoeuvring modeling group
ODE	–	ordinary differential equation
OLS	–	ordinary least squares
PI	–	physics informed model
PMM	–	planar motion mechanism
PU	–	physics uninformed model
RISE	–	research institutes of Sweden
RTS	–	Rauch Tung Striebel smoother
SDT	–	ship digital twin
SI	–	international system of units
SINDy	–	sparse identification of nonlinear dynamics
SSPA	–	SSPA maritime center
SVR	–	support vector regression
VCT	-	virtual captive test
VIF	-	variance inflation factor
WAPS	–	wind-assisted propulsion system
wPCC	–	wind powered car carrier test case

Chapter 1

Introduction

This chapter begins with an overview of the research subject, followed by a literature review that outlines the motivation, objectives, assumptions, and limitations of this study. The chapter concludes with an outline of the thesis.

The term "model" is used frequently throughout this thesis, but its meaning varies across engineering disciplines. This thesis adopts a more precise definition to avoid ambiguity, by distinguishing between "model structure" – defined for mathematical models by "model equations" – and "identified model", which refers to the complete model, including the identified parameters within the model equations.

1.1 Background

The ability to understand and ensure the controllability of vessels is essential for achieving safe marine operations. Ships exceeding 100 meters must meet formal manoeuvring requirements (IMO 2002), which are ultimately verified during sea trials. However, preliminary assessments are often performed before ship construction through ship models. Building a physical-scale model to conduct free-running model tests (FRMT) is still recognized as the most reliable method (ITTC 2008) for benchmarking performance. However, these physical-scale models are often complemented by more abstract approaches, such as numerical models in computational fluid dynamics (CFD) or data-driven models.

"Loosely speaking, a model is a tool we use to answer questions about the system without having to do an experiment" (Ljung et al. 2021). There are many situations where an experiment using a full-scale ship is undesirable; for instance, such experiments may be cost prohibitive, time consuming, inherently dangerous, or simply impossible if the ship has not been built. CFD has been developed to describe the hydrodynamics of ships based on the fundamental principles of physics. However, there are many situations where this is infeasible: calculations may be prohibitively expensive, or perhaps the geometries, calculation domain, or boundary conditions may not be definable with sufficient accuracy. Therefore, in many cases, the lack of a complete physical understanding of the system must be accepted, and instead, a data-driven model is used, which mimics the system behavior based on observations. This thesis explores the use of such data-driven models for manoeuvring.

Model structures for manoeuvring are often categorized in the literature as either parametric models or non-parametric models. A third category, hybrid models, combines parametric and non-parametric models. Parametric models are characterized by a fixed number of parameters, in contrast to non-parametric models that have a flexible number of parameters, which can grow with the size of the data.

There are primarily two approaches used to obtain the necessary data for use in model creation: the captive test (CT) and the free-running test (FT). Both methodologies will be discussed in this thesis. Captive model tests (CMT) are the conventional method for obtaining CT data and can be conducted using various

means, such as with an XY-carriage, a rotating arm, or a planar motion mechanism (PMM). Virtual captive tests (VCT) extend this approach by incorporating CFD simulations. FT data are collected from either model tests, full-scale ship trials, or in some cases, direct CFD (Araki et al. 2012). CT data are generally more applicable in virtual prototyping when assessing the manoeuvring performance before ships are built. In contrast, FT data are typically more applicable to existing ships, in a digital twin context.

The success of system identification methods depends on both the chosen model structure and the quality of the data in terms of measurement accuracy and amount of information. Many studies in the literature discuss system identification of parametric models from simulated data. However, this has been considered an irrelevant scenario in this thesis, since the model structure that generated the data is known beforehand; "we identify real objects, not their mathematical model" (Miller 2021). Nevertheless, the use of simulated data in gauging the ability of a non-parametric model to identify a suitable model structure remains relevant. Although parametric models will be the primary focus of this thesis, other approaches will also be discussed in the subsequent literature review.

1.2 Literature review

This literature review explores papers on the use of data-driven models identified from CT or FT data for the manoeuvring of ship. Papers on parametric, non-parametric, or hybrid models are first briefly introduced in subsection 1.2.1 and 1.2.2. This introduction is followed by a more in-depth review of the models identified from CT or FT data as presented in subsection 1.2.3 and 1.2.4. Papers addressing the system identification of parametric models using simulated data have been deemed irrelevant for this thesis and, consequently, have not been included in this review.

1.2.1 Parametric models

Parametric model structures represent a class of grey-box models where parameterization is based on varying levels of physical insights (greyness) as described by classical manoeuvring models, such as the Nomoto model structure (Nomoto et al. 1957), the Abkowitz model structure (Abkowitz 1964), and the Norrbin model structure (Norrbin 1971). The Nomoto and Abkowitz model structures are both pure mathematical models. The Nomoto model structure characterizes the yaw dynamics of ships and is particularly useful for predicting a ship's response to steering inputs, for instance in autopilot applications. Tzeng and Chen (1999) investigated the fundamental properties associated with the Nomoto model. The Abkowitz model structure describes the total forces acting on a ship in three degrees of freedom as a truncated third-order Taylor expansion. Norrbin (1971) added more physical insight into the model structures; first in the use of second-order modulus functions to model the nonlinearities with coefficients, such as $N_{v|v|}$ and $N_{v|r|}$, later to be replaced by the cross flow drag principle (Fossen 2011). More physical insights were added in the modular model structure of the Manoeuvring Modeling Group (MMG) model structure (Ogawa and

Kasai 1978; Inoue et al. 1981; Yasukawa and Yoshimura 2015). Instead of describing the total force acting on the ship, the model structure was divided into sub models for the propeller, rudder, and hull.

1.2.2 Non-parametric or hybrid models

Advancements in machine learning have enabled the expression of ship manoeuvring through non-parametric models. Non-parametric models may be considered black-box models, which Ljung (2010) describes as flexible function surfaces. Examples of non-parametric models include various types of neural networks (Rajesh and Bhattacharyya 2008; He and Zou 2020; He et al. 2022), support vector machine regression (SVM) (Chen et al. 2023; Zihao Wang et al. 2020), or Gaussian process models (GP) (Zhang and Ren 2021; Xue et al. 2021; Xue et al. 2022).

Non-parametric models provide flexibility, enabling them to represent a wide range of hydrodynamic relationships, whereas parametric models may struggle to capture hydrodynamics accurately in certain cases. However, if the assertion by Revestido Herrero and Velasco González (2012) is correct, "the parametric model structures provide a suitable set of models in which it can be assumed that a true model belongs", this means that the physical insights from the parametric models might also add valuable prior information to the system identification.

Hybrid models have been developed to integrate parametric and non-parametric approaches. Wang et al. (2021) propose a framework in which the foundation is set by the best available parametric model, which is then refined with a neural network. Nielsen et al. (2022) use a similar approach. Dong et al. (2023) combine an MMG model with an SVM corrector.

1.2.3 Captive tests

Identifying a manoeuvring model from CMT or VCT is challenging: "All practical manoeuvring mathematical models are highly schematised and although in principle can be tuned to provide a satisfactory reproduction of the true motion, there are no simple theoretical methods for estimating their parameters" (Sutulo and Guedes Soares 2014). Sutulo and Soares (2004) developed a computer code for planning captive tests with D-optimized experimental designs so that the most precise estimates of model parameters could be obtained with the least number of experimental runs. Sakamoto et al. (2012) showed how added masses could be obtained from dynamic PMM simulations with unsteady Reynolds averaged Navier–Stokes (URANS) computations. Moctar et al. (2014) used a similar approach to determine the added masses. However, Sakamoto et al. (2012) strongly recommended using static tests for damping coefficients, instead of the single-run method applied on dynamic PMM tests. Moctar et al. (2014) identified an Abkowitz model from VCT for a twin-screw dock ship. Simulations with the VCT model were compared to CFD direct manoeuvring simulations and FRMT. Two different ways of modeling the propeller were investigated; the moving reference frame approach was 50 times faster than the sliding interface approach, but less accurate. The VCT model was found to be very efficient and results showed

satisfactory agreement. However, the direct simulations showed better agreement. Hajivand and Mousavizadegan (2015) identified an Abkowitz model from VCT data for the DTMB 5512 model ship. The coefficients were determined from VCT data using a test program as outlined by Yoon et al. (2015) that included oblique towing tests with drift angle variations at three speeds, and PMM tests of pure sway and pure yaw. Simulations could not be compared with FRMT data since such tests were not available for the DTMB 5512 model ship. Instead, a comparison between simulations with models identified from VCT or captive model tests was conducted by Yoon et al. (2015); these were found to be in very good agreement.

Liu et al. (2018) identified an Abkowitz model from VCT data for the KCS container ship. Zigzag simulations with the identified model were compared with corresponding FRMT data (SIMMAN 2014). The simulations were also compared with previous simulations conducted by Simonsen (2014) with a different model structure. This model structure was identified from both VCT and standard PMM model tests. The underprediction of zigzag overtshoot angles from all these simulations in relation to the FRMTs are summarized in Table 1.1, where VCT A denotes the results from Liu et al. (2018) and VCT B and PMM B are the results from Simonsen (2014) with the models obtained from either the VCT or PMM model tests. Since all values in this table are positive,t follows that all of the simulations underpredicted the FRMT overhoot angles. It would be reasonable to assume that the PMM model tests have the ability to provide a correct physical representation of the hydrodynamics in the FRMT. However, agreement between the PMM B simulations and the FRMT was not perfect. It seems that the accuracy of the model does not only depend on the accuracy of the CT data, but may also depend on which model structure is used and how the states are varied to identify the parameters.

Table 1.1: Under predictions from the simulated overshoot angles (deg) in relation to FRMTs as reported in Liu et al. (2018)

Zigzag	Overshoot	VCT A	VCT B	PMM B
10	first	1	3	3
10	second	4	7	7
20	first	7	7	7
20	second	4	3	5

1.2.4 Free running tests (system identification)

Models are often tuned manually before being implemented in bridge simulators, although such approaches are rarely mentioned in the literature (Sutulo and Guedes Soares 2014). More structured approaches to system identification for parametric models typically involve some form of Kalman filter (KF) in the process. The use of a KF combined with maximum likelihood estimation was proposed in 1976 by Åström and Källström (1976) to identify a linear manoeuvring model that utilized manually recorded data aboard the Atlantic Song freighter. Currently, the extended

Kalman filter (EKF) is the predominant system identification method. It is used to estimate ship state from noisy data during manoeuvres, but it can also estimate model parameters as shown by Shi et al. (2009) and Perera et al. (2015). In this approach, the parameters are updated continuously so that the model can adapt over time in real-time. This approach is quite challenging for larger model structures where many parameters need to be simultaneously estimated. Instead, Yoon and Rhee (2003) introduced an estimation-before-modeling technique (two-step approach), also used by Revestido Herrero and Velasco González (2012), where only the state of the ship is estimated by EKF and the model parameters are identified by another method. Some studies in the literature have not used the EKF: Tiano and Blanke (1997) used a random search minimization method and also included roll motion in the system identification; Casado and Ferreiro (2005) used the backstepping procedure and the tuning design method; and Miller (2021) used a genetic algorithm to identify parameters. Additionally, Chillcce and Moctar (2023) used numerical calculations of velocities and accelerations by applying the Savitzky–Golay numerical differentiation method (Ahnert and Abel 2007), instead of the EKF. They used an Euler equation-based numerical approach (Moctar et al. 2022) to determine the zero-frequency added masses and a constrained least-squares algorithm for linear regression, akin to the approach by Araki et al. (2012).

Multicollinearity in statistical modeling describes a scenario where two or more predictor variables are highly correlated, making it difficult to isolate the individual effects of each predictor on the dependent variable. This issue is particularly relevant in the field of ship manoeuvring modeling, where numerous hydrodynamic coefficients and parameters are involved. The higher the correlation between the regression variables, or the stronger the multicollinearity, the more difficult it is to identify the regression coefficients separately (Yoon and Rhee 2003). Wang and Zou (2018) analyzed the effects of multicollinearity on parameter drift in system identification. They showed that when predictor variables are highly correlated, the estimates of the model parameters can become unstable and sensitive to small changes in the data. in their work, the variance inflation factor (VIF) was used to quantify the severity of multicollinearity in ship manoeuvring models. VIF measures how much the variance of a regression coefficient is inflated due to multicollinearity; a high VIF indicates a high level of multicollinearity. Multicollinearity can be partially mitigated by pre-processing the data. Luo et al. (2016) addressed the issue of parameter identifiability in ship manoeuvring modeling. This study aimed to reconstruct samples and reduce multicollinearity by employing methods such as the difference method and the additional signal method, thereby improving the feasibility of system identification. Xu et al. (2019) introduced methods to address the uncertainty caused by multicollinearity, such as truncated singular value decomposition and Tikhonov regularization. These techniques help in stabilizing the parameter estimates and improving the robustness of the model.

Model structure selection is a more pragmatic approach to addressing multicollinearity, by reducing the number of parameters in the model, ensuring that they are identifiable from the available data. Luo et al. (2016) reduced the number of param-

eters based on physical considerations. Costa et al. (2021) applied truncated singular value decomposition, while Liu et al. (2024) used sparse identification of nonlinear dynamics (SINDy) (Brunton et al. 2016), to reduce the number of model parameters. Abkowitz (1980) addressed multicollinearity through elimination of "inconvenient" terms; however, this approach could lead to models with limited applicability, as certain regression terms may only become significant under specific conditions, such as sailing in wind. This is perhaps the key limitation of model structure selection – that the generalization of a model may suffer when parameters are excluded.

The most effective approach to mitigating multicollinearity is to obtain more informative data with sufficient persistence of excitation. This requires input signals in system identification to be rich in frequency content, ensuring that all system modes are adequately excited. This ensures that the system's response contains enough information to uniquely identify the system parameters. Without persistence of excitation, the identified model may not accurately represent the ship's behaviour in all scenarios.

Yoon and Rhee (2003) discussed the importance of designing experiments that ensure persistence of excitation. They suggested using specific input scenarios that maximize the information content of the data, such as D-optimal designs. An optimal experimental design is easier to obtain for captive tests, where the state of the ship can be varied freely. Although Wang et al. (2020) and Miller (2021) suggested that a pseudo-random sequence (PRS) can be used for free running tests. However, data from these kinds of tests are very rare. A model basin is too small, and full-scale tests of this kind are also very rare. Data for the mandatory zigzag and turning circle standard manoeuvres (IMO 2002) are much more readily available, which explains the frequent use of standard manoeuvres for system identification in many studies in the literature. However, these manoeuvres are not sufficiently rich to guarantee reliable estimation of all regression coefficients (Sutulo and Guedes Soares 2014), which poses a substantial challenge for system identification.

1.3   Motivation and objective

System identification of parametric models has been conducted since the late 1970s using free-running tests, and even longer with captive tests. The first papers on non-parametric models were published in the late 1990s, and their popularity has increased over the past 15 years, particularly in the field of autonomous vessels. Today, research continues to be published on both approaches, indicating no clear consensus on which is superior. New findings continue to emerge on how to improve these models and combine them into hybrid models.

Further advancements in machine learning are expected in the coming years, promising a bright future for non-parametric models and hybrid approaches. However, challenges remain, such as the lack of informative data and persistence of excitation, which are crucial for developing physically accurate models with good generalization capabilities, performing well on new and unseen data.

One often overlooked aspect of indirect informative data is the prior knowledge

of ship hydrodynamics from previous experimental work and other physical insights. These indirect data are frequently embedded in parametric model structures, where the inclusion or exclusion of parameters is often based on careful consideration of experimental results or physical reasoning. Additionally, semi-empirical formulas in the literature could potentially be used to enhance the informative data. This area requires further investigation, which motivates the research question of this thesis as follows:

> *How can prior knowledge embedded in parametric model structures and semi-empirical formulas be used to identify physically correct ship manoeuvring models, with good generalization?*

The research question has been divided into research objectives in Table 1.2 to provide a clear path through this study. The first two objectives (A–B) constitute a prestudy, initially simplifying the problem to consider only one degree of freedom in ship roll motion, which was addressed in Paper 1. Objectives C–D expand this work to include identification and parametric models for the three-degrees-of-freedom manoeuvring problem. Parameter identification techniques for CT and FT data were developed in Papers 3 and 5, respectively. Parametric model structures were proposed in Paper 3, focusing on generalizing from simpler to more complex manoeuvres. The ability of these models to generalize to wind conditions was studied in Paper 4. Further work to develop physically accurate models was carried out in Paper 5, which involved extensive VCT calculations and FT inverse dynamics. Semi-empirical formulas were introduced in Paper 2 for roll damping and in Paper 4 for rudder forces.

Table 1.2: Research objectives of this thesis A–E including sub objectives 1–3 and the appended papers 1–5 where the objectives are mainly addressed.

	Objective	1	2	3	4	5
A	Developing parameter identification techniques for roll motion models from FT data.	✓				
B	Proposing a parametric model structure for roll motion dynamics with good generalization based on prior knowledge from model tests.	✓				
C	Developing parameter identification techniques for ship manoeuvring models from:					
1	FT data.			✓		
2	CT data.					✓
D	Proposing a parametric model structure with good generalization that is identifiable from standard maneuvers.					
1	Generalize from simpler to more complicated manoeuvres.			✓		
2	Generalize to wind conditions.				✓	
3	Physical insights from CFD and FT inverse dynamics.					✓
E	Using semi-empirical formulas to improve generalization.		✓		✓	

1.4   Assumptions and limitations

The following assumptions are made in this thesis.

  (I) Under the rigid body assumption, the ship is modeled as a rigid body that does not deform under the influence of forces.

 (II) Calm water with no external waves is assumed within manoeuvring. The models in this thesis can therefore be described by state-space models with the Markov property, which means that fluid memory effects have been neglected (Fossen 2011).

(III) The maneuvers are assumed to have low-frequency motions, allowing the added masses to be treated as constant values (Fossen 2011).

 (IV) Only experimental data from standard test types, such as turning circles or zigzag tests, are used in this thesis, since they are commonly available for ships.

  (V) Uncertainties related to the measurement data from model scale tests and CFD methods have not been studied, which could be a source of error that is not addressed in this thesis.

 (VI) Free-surface effects were neglected in the VCT calculations, assuming that the wave generation is small or has little influence on the manoeuvring performance.

(VII) Three degrees of freedom are assumed sufficient to describe the manoeuvring dynamics, neglecting influence of roll, heave, and pitch.

1.5   Outline of the thesis

Chapter 2 presents the parametric model structures used in this thesis, including the force prediction submodules for the hull, rudder, and propeller. The methods involved in parameter identification are detailed in chapter 3, covering inverse dynamics, added mass estimation, and the proposed method for recursive inverse dynamics regression. The papers attached to this thesis are summarized in chapter 4, followed by a discussion (chapter 5), conclusions (chapter 6), and comments on future work (chapter 7).

Model structures

Parametric model structures for ship roll motion and manoeuvring are presented in this chapter. Model structures for roll are first introduced in section 2.1. Ship kinematics during manoeuvres is introduced in section 2.2 with force models for the hull (section 2.4), rudders (section 2.5), and propellers (section 2.6).

2.1 Roll motion

The spring-mass-damper system, as shown in Figure 2.1, is a second-order linear ordinary differential equation (ODE) (Eq. (2.1)) that describes the motion of a mass attached to a spring and a damper. It is useful for understanding oscillatory and damping behavior.
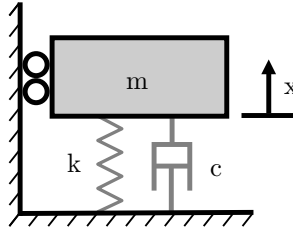
Figure 2.1: Mass-spring-damper model structure.

$$m\ddot{x} + c\dot{x} + kx = 0 \tag{2.1}$$

Roll motion without manoeuvres or external forces can be expressed by a nonlinear spring-mass-damper system (Himeno 1981),

$$A_{44}\ddot{\phi} + \mathrm{B}_{44}\left(\dot{\phi}\right) + \mathrm{C}_{44}\left(\phi\right) = 0 \tag{2.2}$$

where the subscript 44 indicates forces in the roll degree of freedom and the static stability of the ship is expressed as the stiffness $C_{44}(\phi)$ as a function of the roll angle ϕ, the damping $(B_{44}(\dot{\phi}))$ as a function of the roll velocity $\dot{\phi}$, and inertia A_{44} connected to the roll acceleration $\ddot{\phi}$. The ship's roll motion can be observed under these conditions in a roll-decay test. The model is forced to an initial roll angle, as seen in Figure 2.2a. It is then released (Figure 2.2b) and returns to equilibrium (Figure 2.2c). The model will pass the static water line as a result of its momentum and not stop until it has reached the end point on the other side (Figure 2.2d). This motion starts a new cycle, with the model rolling back once more. This new cycle results in oscillatory motion where potential energy is transferred to kinetic energy and back again to potential energy. This oscillation would never end if it were not for the roll damping. Interactions between the ship and the water, such as friction, wave generation, eddy generation, and hydrodynamic lift, cause the ship to lose some

of its energy. This energy loss causes the oscillation to decay over time, as seen in Figure 2.3, which displays the time series for the roll angle.

(a) The ship model is forces to an initial angle and then released

(b) Starts to roll back

(c) Static water line.

(d) End point other side
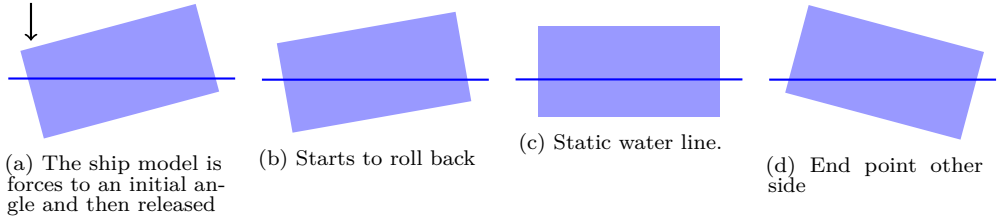
Figure 2.2: Roll decay test.
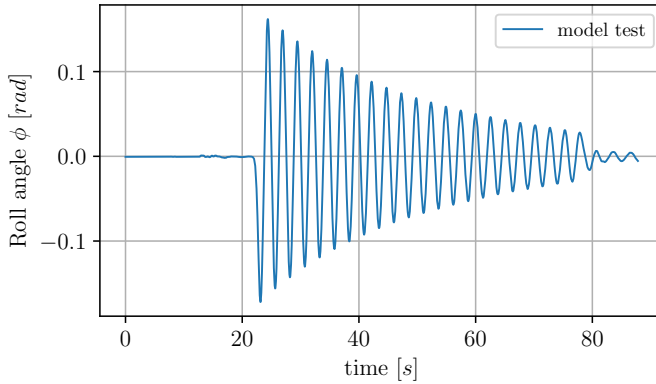
Figure 2.3: Example roll decay signal.

The damping, $B_{44}\left(\dot{\phi}\right)$, can be expressed as an expansion series:

$$B_{44}\left(\dot{\phi}\right) = B_1 \cdot \dot{\phi} + B_2 \cdot \dot{\phi}\left|\dot{\phi}\right| + B_3 \cdot \dot{\phi}^3 + ... + B_n \cdot \dot{\phi}^n \tag{2.3}$$

This series can be truncated, allowing it to be expressed as a "linear model" (Eq. (2.4)), "quadratic model" (Eq. (2.5)), and "cubic model" (Eq. (2.6)). The stiffness function, $C_{44}(\phi)$, has been similarly expanded, only retaining the first term for the linear and quadratic models and the first three terms for the cubic model.

$$A_{44}\ddot{\phi} + B_1\dot{\phi} + C_1\phi = 0 \tag{2.4}$$

$$A_{44}\ddot{\phi} + C_1\phi + \left(B_1 + B_2\left|\dot{\phi}\right|\right)\dot{\phi} = 0 \tag{2.5}$$

$$A_{44}\ddot{\phi} + \left(B_1 + B_2\left|\dot{\phi}\right| + B_3\dot{\phi}^2\right)\dot{\phi} + \left(C_1 + C_3\phi^2 + C_5\phi^4\right)\phi = 0 \tag{2.6}$$

2.2 Manoeuvring

Ship manoeuvring dynamics can be expressed using a state-space model,

$$\dot{\mathbf{x}} = f(\mathbf{x}, \mathbf{c}) + q(t) \tag{2.7}$$

where the change of state, $\dot{\mathbf{x}}$, is expressed as a function of the current state vector, $\mathbf{x}$, and the control input vector, $\mathbf{c}$, through the transition function, $f(\mathbf{x}, \mathbf{c})$, and the process noise $q(t)$. Process noise is considered when the model is used for filtering. However, during deterministic simulations, it is usually set to zero ($q(t) = 0$). A state with position and orientation, velocities, and turning rate defines the state of the ship in three degrees of freedom:

$$\mathbf{x} = [x_0, y_0, \Psi, u, v, r]^T \tag{2.8}$$

The ship's kinematics are expressed amidship in a ship fixed reference frame, rotated around the Earth-fixed axis, x_0, by the heading angle, Ψ (Figure 2.4). Forces and motions are expressed in degrees of freedom of surge, sway, and yaw with forces X, Y, and moment N, as well as the velocities u, v, and r. Kinematics can be expressed as a function of a velocity vector $\boldsymbol{v}$, since forces do not depend on position (x_0, y_0) or direction Ψ, during the maneuver:

$$\boldsymbol{v} = \begin{bmatrix} u \\ v \\ r \end{bmatrix} \tag{2.9}$$

The equation of motion can thus be expressed as:

$$\mathbf{F} = \mathbf{M}\dot{\boldsymbol{v}} \tag{2.10}$$

where $\dot{\boldsymbol{v}}$ is the acceleration vector, $\mathbf{M}$ is the system inertia matrix and $\mathbf{F}$ is the total force vector. The velocity transition can thus be expressed as:

$$\dot{\boldsymbol{v}} = \mathbf{M}^{-1}\mathbf{F} \tag{2.11}$$

The total forces can be divided into the Coriolis–centripetal matrix, $\mathbf{C}$, and the damping force vector, $\mathbf{D}$ (Fossen 2011). The control forces of the rudder and propeller are included in the matrix $\mathbf{D}$.

$$\mathbf{F} = -\mathbf{C}\boldsymbol{v} + \mathbf{D} \tag{2.12}$$

$\mathbf{M}$ and $\mathbf{C}$ are calculated as shown below:

$$\mathbf{M} = \begin{bmatrix} -X_{\dot{u}} + m & 0 & 0 \\ 0 & -Y_{\dot{v}} + m & -Y_{\dot{r}} + mx_G \\ 0 & -N_{\dot{v}} + mx_G & I_z - N_{\dot{r}} \end{bmatrix} \tag{2.13}$$

$$\mathbf{C} = \begin{bmatrix} 0 & -mr & Y_{\dot{r}}r + Y_{\dot{v}}v - mrx_G \\ mr & 0 & -X_{\dot{u}}u \\ -Y_{\dot{r}}r - Y_{\dot{v}}v + mrx_G & X_{\dot{u}}u & 0 \end{bmatrix} \tag{2.14}$$
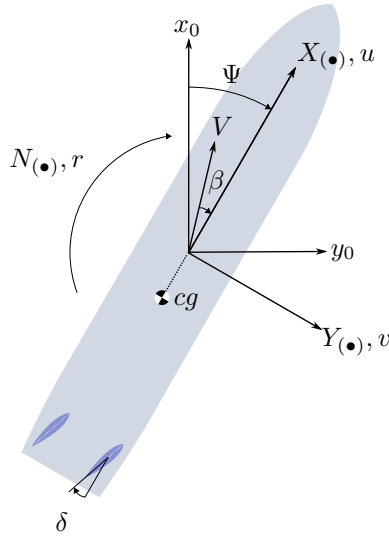
Figure 2.4: Relations between the earth fixed and ship fixed reference frames, showing the velocities and forced in the ship fixed frame.

where the added masses $X_{\dot{u}}, Y_{\dot{v}}, Y_{\dot{r}}, N_{\dot{v}}, N_{\dot{r}} < 0$.

If we introduce the damping forces vector:

$$\mathbf{D} = \begin{bmatrix} X_D \\ Y_D \\ N_D \end{bmatrix} \tag{2.15}$$

the total force vector, $\mathbf{F}$, can now be expressed as:

$$\mathbf{F} = \begin{bmatrix} X \\ Y \\ N \end{bmatrix} = \begin{bmatrix} X_D - Y_{\dot{r}}r^2 + mr^2 x_G + rv\left(-Y_{\dot{v}} + m\right) \\ Y_D + ru\left(X_{\dot{u}} - m\right) \\ N_D + ru\left(Y_{\dot{r}} - mx_G\right) + \underbrace{uv\left(-X_{\dot{u}} + Y_{\dot{v}}\right)}_{\text{Munk moment}} \end{bmatrix} \tag{2.16}$$

Note:

The yawing moment N has the so-called Munk moment (Fossen 2011):

$$uv\left(-X_{\dot{u}} + Y_{\dot{v}}\right)$$

In many other manoeuvring models, such as the Abkowitz model (Abkowitz 1964) or MMG model (Yasukawa and Yoshimura 2015), the Munk moment is not explicitly included in the equations. The Munk moment contribution is instead reflected in some of the hull coefficients, typically N_V or ideally N_{uv}, if such coefficients exist in the model.

Note:

> The sway force Y includes the apparent centrifugal force from added mass and rigid body mass:
>
> $$ru\left(X_{\dot{u}} - m\right)$$
>
> where $X_{\dot{u}} < 0$ so that both added mass and rigid body mass create the centrifugal force acting outward in the turn. Both the added mass and rigid body mass will thus act to starboard on a port turn.

For the calculation of acceleration Eq. (2.11), the inverse of the mass matrix $\mathbf{M}$ can be calculated as:

$$\mathbf{M}^{-1} = \begin{bmatrix} \frac{1}{-X_{\dot{u}}+m} & 0 & 0 \\ 0 & \frac{-I_z+N_{\dot{r}}}{S} & \frac{-Y_{\dot{r}}+mx_G}{S} \\ 0 & \frac{-N_{\dot{v}}+mx_G}{S} & \frac{Y_{\dot{v}}-m}{S} \end{bmatrix} \tag{2.17}$$

with the helper variable, S, which can be calculated according to:

$$S = I_z Y_{\dot{v}} - I_z m - N_{\dot{r}} Y_{\dot{v}} + N_{\dot{r}} m + N_{\dot{v}} Y_{\dot{r}} - N_{\dot{v}} m x_G - Y_{\dot{r}} m x_G + m^2 x_G^2 \tag{2.18}$$

Note that $S = 0$ would mean that the mass matrix would not be invertible. The sign of each component in Eq. (2.18) is shown in:

$$S = -\left|I_z Y_{\dot{v}}\right| - \left|I_z m\right| - \left|N_{\dot{r}} Y_{\dot{v}}\right| - \left|N_{\dot{r}} m\right| + \left|N_{\dot{v}} Y_{\dot{r}}\right| + \left|m^2 x_G^2\right| + \left|N_{\dot{v}} m x_G\right| + \left|Y_{\dot{r}} m x_G\right| \tag{2.19}$$

The magnitude of these components for a typical ship is expressed in a non-dimensional form in Table 2.1. The negative components are much larger than the positive, so S will be nonzero and the mass matrix of a ship is thus always invertible.

Table 2.1: Signs and magnitudes of the components within helper variable S for a typical ship in non-dimensional form.

part	magnitude
$-\left|I_z Y_{\dot{v}}\right|$	-1e-05
$-\left|I_z m\right|$	-1e-05
$-\left|N_{\dot{r}} Y_{\dot{v}}\right|$	-1e-05
$-\left|N_{\dot{r}} m\right|$	-1e-05
$\left|N_{\dot{v}} Y_{\dot{r}}\right|$	1e-07
$\left|m^2 x_G^2\right|$	1e-07
$\left|N_{\dot{v}} m x_G\right|$	1e-07
$\left|Y_{\dot{r}} m x_G\right|$	1e-07

2.3 Prime system with perturbed surge velocity

Some variables in the equations in this thesis are expressed using non-dimensional units with the prime system, denoted by the prime symbol ($'$). Variables are converted from SI units to the prime system using the denominators in Table 2.2 for the corresponding physical quantity, where V and L are the velocity and length between the perpendiculars of the ship, respectively, and ρ is the water density. For the calculation of surge velocity, u', the perturbed velocity, $(u - V_0)$, about a nominal speed, V_0, is used, as in Eq. (2.20), to avoid a u' of 1 for all speeds when the ship is on a straight course (where $u = V$), as in a resistance or self-propulsion test. The usage of the perturbed velocity, therefore, allows for higher-order resistance terms in the model, such as $dX'/du' = X_u$, which are otherwise not possible.

$$u' = \frac{u - V_0}{V} \tag{2.20}$$

For a non-dimensional model, V_0 is instead expressed as a Froude number within the model (Eq. (2.21)), and this thesis uses $F_{n0} = 0.02$.

$$F_{n0} = \frac{V_0}{\sqrt{g \cdot L}} \tag{2.21}$$

Table 2.2: Scalings with prime system.

Physical quantity	SI unit	Denominator
length	m	L
volume	m^3	L^3
mass	kg	$\frac{L^3\rho}{2}$
density	kg/m^3	$\frac{\rho}{2}$
inertia moment	kg m^2	$\frac{L^5\rho}{2}$
time	s	$\frac{L}{V}$
frequency	1/s	$\frac{V}{L}$
area	m^2	L^2
angle	rad	1
linear velocity	m/s	V
angular velocity	rad/s	$\frac{V}{L}$
linear acceleration	m/s^2	$\frac{V^2}{L}$
angular acceleration	rad/s^2	$\frac{V^2}{L^2}$
force	N	$\frac{L^2V^2\rho}{2}$
moment	Nm	$\frac{L^3V^2\rho}{2}$

2.4 Hull model

Hull forces are described by the following general polynomials, which are expressed in prime system units (see section 2.3). The associated parameters express hydrodynamic derivatives, such as $X'_{vr} = dX'/(dv'dr')$. The perturbed surge velocity allows for the extra resistance term, X_u', so the resistance curve does not need to be quadratic as in the MMG model (Yasukawa and Yoshimura 2015).

$$X'_H = X'_0 + X'_{rr}r'^2 + X'_u u' + X'_{vr}r'v' + X'_{vv}v'^2 \tag{2.22}$$

$$Y'_H = Y'_0 + Y'_{rrr}r'^3 + Y'_r r' + Y'_{vrr}r'^2 v' + Y'_{vvr}r'v'^2 + Y'_{vvv}v'^3 + Y'_v v' \tag{2.23}$$

$$N'_H = N'_0 + N'_{rrr}r'^3 + N'_r r' + N'_{vrr}r'^2 v' + N'_{vvr}r'v'^2 + N'_{vvv}v'^3 + N'_v v' \tag{2.24}$$

2.5 Rudder models

It has become evident during this investigation that an accurate rudder model is central to achieving high accuracy in the overall manoeuvring model. Polynomial rudder models were used in Paper 3, which well describe the rudder forces if a sufficiently high polynomial degree is used. However, these models introduce multicollinearity into the model, which poses a significant challenge in system identification, particularly when estimating parameters using inverse dynamics (see section 3.6). Since only the total force acting on the ship can be observed, it becomes difficult to separate hull-generated forces from rudder-induced forces as shown in Figure 2.5. Instead of using a data-driven rudder model, a semi-empirical deterministic rudder model (see subsection 2.5.1) was therefore introduced in Paper 4. The rudder forces were calculated on the basis of the rudder's characteristics and established coefficients from the literature. A third rudder model was introduced in Paper 5 as a modified version of the MMG rudder model (Yasukawa and Yoshimura 2015). This model was found to be easier to adopt when very rich information about the rudder forces was available from the VCT data.

2.5.1 Semi-empirical rudder model

The semi-empirical rudder model was proposed in Paper 4 as is a lifting-line model, similar to Hughes et al. (2011), Matusiak (2021), and Kjellberg et al. (2023), which is primarily based on the rudder wind tunnel tests conducted by Whicker and Fehlner (1958). The surge and sway forces are expressed as rudder lift L_R and rudder drag D_R, which are projected on the ship through the rudder inflow angle α_f (see Eq. (2.25), Eq. (2.26), and Figure 2.6). This angle is the sum of the initial inflow to the rudder at a straight course γ_0 and the inflow to the rudder γ due to propeller-induced speed, drift angle, and yaw rate of the ship, as shown in Eq. (2.28).

$$X_R = -D_R \cos(\alpha_f) + L_R \sin(\alpha_f) \tag{2.25}$$

$$Y_R = D_R \sin(\alpha_f) + L_R \cos(\alpha_f) \tag{2.26}$$
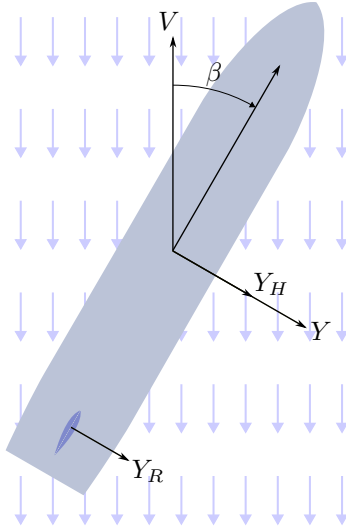
Figure 2.5: Multicollinearity between hull and rudder forces.
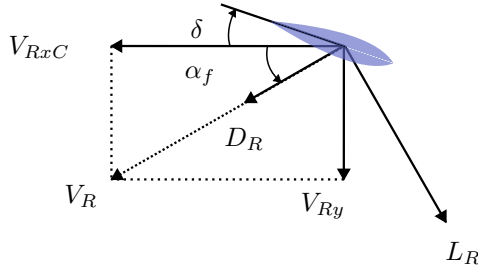
Figure 2.6: Inflow to the rudder.

$$\alpha_f = \gamma_0 + \gamma \tag{2.27}$$

$$\gamma = \text{atan}\left(\frac{V_{Ry}}{V_{RxC}}\right) \tag{2.28}$$

The transverse velocity in the rudder V_{Ry} is calculated by multiplying the yaw rate of the ship r and the transverse velocity v by their flow straightening parameters κ_{rtot} and κ_{vtot} (Eq. (2.29)). These parameters have linear and nonlinear dependencies on the geometric inflow angle, γ_g (Eq. (2.32)), as calculated in Eq. (2.30) with $\kappa_r, \kappa_{r\gamma g}$ and Eq. (2.31) with $\kappa_v, \kappa_{v\gamma g}$, respectively, so the flow straightening may vary for different inflow angles. Linear and nonlinear dependencies were determined from the VCT rudder forces. A detailed calculation of the axial velocity on the rudder V_{RxC}, including the propeller race velocity, is presented in Paper 4.

$$V_{Ry} = -\kappa_{rtot}rx_R - \kappa_{vtot}v \tag{2.29}$$

$$\kappa_{rtot} = \kappa_r + \kappa_{r\gamma g} |\gamma_g| \tag{2.30}$$

$$\kappa_{vtot} = \kappa_v + \kappa_{v\gamma g} |\gamma_g| \tag{2.31}$$

$$\gamma_g = \text{atan} \left(\frac{-rx_R - v}{V_{RxC}} \right) \tag{2.32}$$

The yawing moment is modeled as the sway force multiplied by the lever arm x_R, as in Eq. (2.33).

$$N_R = Y_R x_R \tag{2.33}$$

Rudder lift

Inspired by work conducted by Villa et al. (2020), the total rudder lift is calculated as the sum of the lift at the rudder areas that are covered by the propeller L_{RC} and that at the uncovered area L_{RU}, as shown in Eq. (2.34) and Figure 2.7.

$$L_R = L_{RC} + L_{RU} \tag{2.34}$$

The lift forces are calculated (Eq. (2.35) and Eq. (2.36)) with the lift coefficient, C_L. These equations are essentially the same except that the lift at the covered area, L_{RC}, is diminished by the factor λ_R (see Paper 4) because of the limited radius of the propeller slipstream in the lateral direction (Brix 1993).

$$L_{RU} = \frac{A_{RU} C_L V_{RU}^2 \rho}{2} \tag{2.35}$$

$$L_{RC} = \frac{A_{RC} C_L V_{RC}^2 \lambda_R \rho}{2} \tag{2.36}$$

See Paper 4 for details on the calculation of the uncovered V_{RU} and covered V_{RC} velocities.
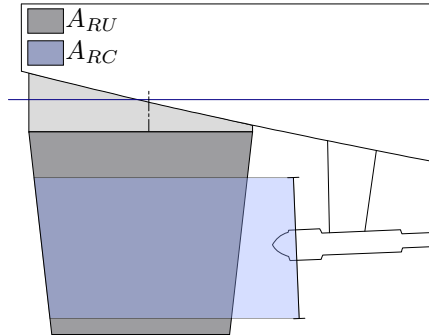
Figure 2.7: Rudder areas covered and uncovered by the propeller.

The lift coefficient, C_L, for a non-stalling rudder is calculated according to Whicker and Fehlner (1958), with the additional parameter K_{gap}, as shown in Eq. (2.37).

$$C_L = K_{gap} \left(\alpha \frac{\partial C_L}{\partial \alpha} + \frac{C_{DC} \alpha |\alpha|}{AR_e} \right) \tag{2.37}$$

$$\alpha = \delta + \gamma_0 + \gamma \tag{2.38}$$

The effective aspect ratio, AR_e, accounts for the mirror image effect when the rudder is flush with the hull, and it is typically assumed to be twice the geometric aspect ratio, AR_g (Eq. (2.40) and Eq. (2.39)) (Hughes et al. 2011). However, the wPCC rudder is not flush with the hull, so a gap is created between the rudder and rudder horn at larger rudder angles, reducing the pressure difference between the high- and low-pressure sides in the upper region of the rudder. Matusiak (2021) proposed that the gap effect can be modeled as a reduced aspect ratio. Instead, this thesis opts for a more straightforward approach based on experience. A factor, K_{gap}, is introduced, calculated according to Eq. (2.41). The gap effect is only activated above a threshold rudder angle, δ_{lim}, and the strength of the gap effect is modeled by a factor, s, as in Figure 2.8.

$$AR_g = \frac{b_R^2}{A_R} \tag{2.39}$$

$$AR_e = 2AR_g \tag{2.40}$$

$$K_{gap} = \begin{cases} 1 & \text{for } \delta_{lim} > |\delta| \\ s\left(-\delta_{lim} + |\delta|\right)^2 + 1 & \text{otherwise} \end{cases} \tag{2.41}$$
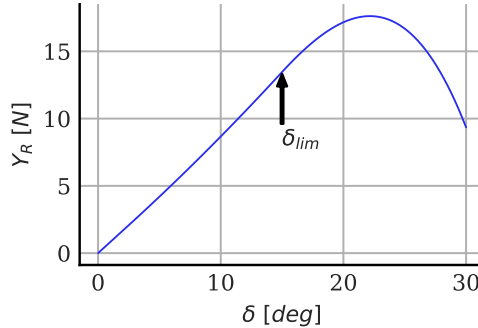
Figure 2.8: Rudder lift is reduced by the gap between the rudder and rudder horn for larger rudder angles.

The lift slope of the rudder $\frac{\partial C_L}{\partial \alpha}$ is calculated using Eq. (2.42), where a_0 is the section lift curve slope (Eq. (2.43)) and Ω is the sweep angle of the quarter chord line (Lewis 1989).

$$\frac{\partial C_L}{\partial \alpha} = \frac{AR_e a_0}{\sqrt{\frac{AR_e^2}{\cos^4(\Omega)} + 4}\cos(\Omega) + 1.8} \tag{2.42}$$

$$a_0 = 1.8\pi \tag{2.43}$$

Additionally, a small nonlinear component of C_L is modeled by the cross-flow drag coefficient C_{DC}, which is calculated for a rudder with a squared tip using Eq. (2.44),

where the taper ratio λ is the ratio between the chords at the tip and the root of the rudder (Eq. (2.45)) (Hughes et al. 2011).

$$C_{DC} = 1.6\lambda + 0.1 \tag{2.44}$$

$$\lambda = \frac{c_t}{c_r} \tag{2.45}$$

Rudder drag

The total rudder drag, D_R, is calculated as the sum of the contributions from the parts covered and uncovered by the propeller, as in Eq. (2.46).

$$D_R = 0.5\rho \left(A_{RC} C_{DC} V_{RC}^2 + A_{RU} C_{DU} V_{RU}^2 \right) \tag{2.46}$$

See Paper 4 for a detailed explanation of the calculation of the drag coefficients, C_{DC} and C_{DU}.

2.5.2 Modified quadratic MMG rudder model

A modified quadratic MMG rudder model is proposed in Paper 5 featuring two enhancements to the original MMG rudder model (Yasukawa and Yoshimura 2015). The first enhancement involves adding the rudder initial inflow angle, γ_0, to the calculation of the effective inflow angle to the rudder, α_R, by replacing Equation 21 in Yasukawa and Yoshimura (2015) with the modified equation (Eq. (2.47)). This allows the rudder model to produce a side force in the straight ahead condition, due to asymmetrical flow from the propeller.

$$\alpha_R = \delta + \underbrace{\gamma_0}_{\text{proposed}} + \operatorname{atan}\left(\frac{v_R}{u_R} \right) \tag{2.47}$$

The rudder transverse velocity, v_R, is calculated as:

$$v_R = V\beta_R\gamma_R \tag{2.48}$$

where β_R is the effective inflow angle to the rudder as a function of both the drift angle, β, and yaw rate, r:

$$\beta_R = \beta - \frac{l_R r}{V} \tag{2.49}$$

where l_R is a lever arm to the rudder that is treated as an experimental constant. The other enhancement specifies a quadratic relationship between the flow straightening coefficient, γ_R, and the effective inflow angle, β_R, by introducing two new coefficients (γ_{R2neg} and γ_{R2pos}), as shown in:

$$\gamma_R = \begin{cases} \overbrace{\gamma_{R2neg} \left| \beta_R \right|}^{\text{proposed}} + \gamma_{Rneg} & \text{for } \beta_R \leq 0 \\ \gamma_{R2pos} \left| \beta_R \right| + \gamma_{Rpos} & \text{otherwise} \end{cases} \tag{2.50}$$

2.6 Propeller model

The surge forces from the propeller are taken as the propeller thrust multiplied by a thrust deduction factor t_{df}:

$$X_P = (1 - t_{df})T \tag{2.51}$$

The propeller thrust T is taken as the measured thrust from VCT or FRMTs in this thesis to reduce the uncertainty associated with the complex interactions involving the propeller, rudder, and hull. The propeller also generates side forces, especially for yaw rates, which have a small stabilizing effect on the ship. This stabilizing propeller moment can be approximately 5% of the rudder yawing moment, as shown in Figure 2.9. This effect is not explicitly modeled in this thesis, so that $Y_P = 0$, $N_P = 0$. Since the propeller side force is included in the VCT data, it is implicitly incorporated into the hull coefficients.
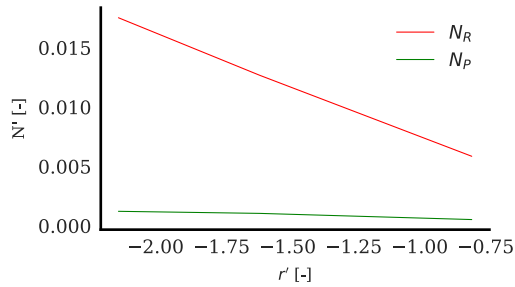
Figure 2.9: Typical yawing moments from rudder and propeller for various yaw rates.

Chapter 3

Parameter estimation

The system identification of rigid body ship dynamics can be reduced to parameter estimation if a parametric model is assumed to be the most appropriate model from a collection of candidate models. Estimating the parameters within the manoeuvring model structure involves estimating the damping parameters within the hull and rudder models, with hydrodynamic derivatives, such as N'_v, Y'_{rrr}, and X'_{vv} (as presented in the previous chapter), in addition to the added masses, so that the equation of motion (Eq. (2.10)) can be evaluated.

A method for estimating added masses is presented in section 3.2. The damping parameters can be estimated directly from the VCT forces as presented in section 3.1. However, this method cannot be used in the FT time series, where the forces cannot be obtained directly. Instead, the forces are estimated through inverse dynamics, which is first introduced for the one-degree-of-freedom roll motion in section 3.3 and then expanded to three-degrees-of-freedom manoeuvring in section 3.4 and section 3.6. Inverse dynamics requires a very accurate description of acceleration, which can be estimated by a Kalman filter, as shown in section 3.5. Filtering and inverse dynamics have been combined into a recursive method, as presented in section 3.7. This chapter concludes with descriptions of the test cases and corresponding data sets used in this thesis in section 3.8 and 3.9.

3.1 Parameter estimation from virtual captive tests

The computational cost of CFD calculations can be significantly reduced by assuming a memory-less state space model (Eq. (2.7)), also known as the Markov process assumption (Yoon and Rhee 2003). This assumption implies that the forces acting on the ship at each time step can be constructed as a series of independent static flow calculations. The independence of these static flow calculations means they are not time-dependent, and their order of computation is irrelevant. The Markov process assumption allows for substantial computational efficiency gains because the ship experiences the same state $\mathbf{x}$ and control input $\mathbf{c}$ (or very similar states and inputs) multiple times during a maneuver. Consequently, the same static flow result can be reused several times, or at least conceptually, this reuse can be considered. Practically, this is achieved by identifying a prediction model for the static flow results, the VCT data, so that forces for each state during the maneuver can be predicted.

One of the challenges in VCT is selecting the appropriate static flow calculations. This involves creating a VCT matrix that includes the most critical states during the maneuver and covers the relevant parts of the state space. The ship's kinematics are defined by the velocity vector $\boldsymbol{v}$ and the control input vector $\mathbf{c}$, allowing the forces for each state to be uniquely defined by the velocities u, v, and r, as well as the control input forces from the rudder and propeller. If these forces are uniquely determined by the thrust and rudder angle, the state space spans at least five dimensions, which requires numerous VCT calculations to cover the entire state space. As a result,

it is difficult to select a model structure in a VCT that closely resembles the true hydrodynamics while ensuring high accuracy, without having to span the entire state space. Table 3.1 and Table 3.2 present the VCT matrices for the wPCC and Optiwise test cases. The coverage of the yaw rate and drift angle space is illustrated by the phase plots in Figure 3.1.

Table 3.1: State variations with VCT for wPCC.

Test type	V [m/s]	β [deg]	r [rad/s]	δ [deg]	rev [1/s]
Circle	0.96		$-0.06 - 0.06$		8.79
Circle + Drift	0.96	$-12 - 12$	$-0.07 - 0.07$		8.79
Circle + Drift + rudder angle	$0.78 - 0.96$	$-13 - 13$	$-0.07 - 0.07$	$-20 - 20$	$7.2 - 8.8$
Circle + rudder angle	0.96		$-0.05 - 0.05$	$-10 - 10$	8.79
Drift angle	0.96	$-15 - 15$			8.79
Rudder and drift angle	0.96	$-4 - 4$		$-10 - 10$	8.79
Rudder angle	0.96			$-15 - 15$	8.79
Thrust variation	$0.48 - 0.96$			$-10 - 10$	$3.8 - 10.0$
self propulsion	$0.48 - 0.96$				$4.6 - 8.8$

Table 3.2: State variations with VCT for Optiwise.

Test type	V [m/s]	β [deg]	r [rad/s]	δ [deg]	rev [1/s]
Circle	0.94		$-0.07 - 0.07$		10.32
Circle + Drift	0.94	$-10 - 10$	$-0.07 - 0.10$		10.32
Circle + Drift + rudder angle	$0.64 - 0.94$	$-10 - 11$	$-0.08 - 0.07$	$-20 - 20$	$7.1 - 10.4$
Circle + rudder angle	0.94		$-0.02 - 0.05$	$-4 - 10$	10.32
Drift angle	0.94	$-10 - 10$			$10.3 - 10.5$
Rudder and drift angle	0.94	$-4 - 7$		$-4 - 10$	10.32
Rudder angle	$0.62 - 0.94$			$-15 - 15$	$7.0 - 10.4$
Thrust variation	$0.62 - 0.94$			$-10 - 10$	$5.8 - 11.3$
self propulsion	$0.62 - 0.94$				$7.0 - 10.3$

(a) wPCC.

(b) Optiwise.
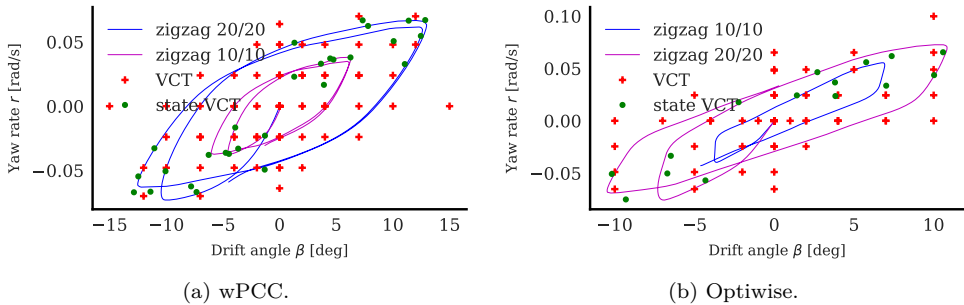
Figure 3.1: Phase plots of the zigzag tests together with the coverage of the VCTs and extra state VCTs.

The hydrodynamic damping forces are calculated from the VCT results X_{VCT},

Y_{VCT}, and N_{VCT} with Eq. (3.1)–Eq. (3.3).

$$X_D = X_{VCT} + Y_{\dot{r}}r^2 + Y_{\dot{v}}rv \tag{3.1}$$

$$Y_D = -X_{\dot{u}}ru + Y_{VCT} \tag{3.2}$$

$$N_D = N_{VCT} + X_{\dot{u}}uv - Y_{\dot{r}}ru - Y_{\dot{v}}uv \tag{3.3}$$

The mass m has been eliminated in Eq. (2.16) to arrive at these expressions, because the ship is stationary in ShipFlow – the CFD tool used in the static flow calculations – and the water experiences either oblique or circular inflow (RoyChoudhury et al. 2017). The hull forces are calculated by subtracting the contributions of the rudder and propeller from the total forces (Eq. (3.4)–Eq. (3.6)).

$$X_H = X_D - X_R - X_P \tag{3.4}$$

$$Y_H = Y_D - Y_R \tag{3.5}$$

$$N_H = N_D - N_R \tag{3.6}$$

These forces are used together with the hull force model (Eq. (2.22) – Eq. (2.24)) to define a linear regression problem that is solved with the ordinary least squares (OLS) method.

3.2 Added mass estimation with the Fourier series method

The yaw added mass $N_{\dot{r}}$ was determined with the Fourier series method (Sakamoto et al. 2021) applied on a pure yaw test conducted in a fully nonlinear potential flow (FNPF) panel method in ShipFlow Motions (Motions) (Kjellberg 2013). During the pure yaw test, the heading Ψ was varied according to Eq. (3.7) so that the yaw rate r and yaw acceleration $\dot{r}$ were varied according to Eq. (3.8) and Eq. (3.9).

$$\Psi = -\Psi_{max} \cos{(tw)} \tag{3.7}$$

$$r = \Psi_{max}w \sin{(tw)} \tag{3.8}$$

$$\dot{r} = \Psi_{max}w^2 \cos{(tw)} \tag{3.9}$$

The pure yaw calculations in Motions were conducted without inclusion of a propeller and rudder so that $N_D = N_H$ and the moment equilibrium with the yawing moment from the pressure integration in Motions N_M could be expressed with Eq. (3.10), where the yaw added mass, $N_{\dot{r}}$, was the coefficient of interest.

$$N_M = N_{\dot{r}}\dot{r} + N_{rrr}r^3 + N_r r + Y_{\dot{r}}ru \tag{3.10}$$

The time series for the yawing moment during the pure yaw test could thus be expressed by inserting Eq. (3.7)–Eq. (3.9) into Eq. (3.10), as shown in Eq. (3.11).

$$\begin{aligned} N_M = N_{\dot{r}}\Psi_{max}w^2 \cos{(tw)} + N_{rrr}\Psi_{max}^3 w^3 \sin^3{(tw)}+ \\ N_r\Psi_{max}w \sin{(tw)} + Y_{\dot{r}}\Psi_{max}uw \sin{(tw)} \end{aligned} \tag{3.11}$$

Eq. (3.11) can instead be expressed as a Fourier series with three components, as shown in Eq. (3.12), where $N_{\dot{r}}$ can be calculated from the first cosine coefficient (Eq. (3.13)).

$$N_M = N_0 + \sum_{n=1}^{3} a_n \cos(n\omega t) + \sum_{n=1}^{3} b_n \sin(n\omega t) \tag{3.12}$$

$$N_{\dot{r}} = \frac{a_1}{\Psi_{max}\omega^2} \tag{3.13}$$

An example of the fitted Fourier series is shown in Figure 3.2. The sway added mass, $Y_{\dot{v}}$, was similarly determined with a pure sway test. The coupled added masses, $N_{\dot{v}}$ and $Y_{\dot{r}}$, were determined with strip theory calculations using Frank's close fit method.

(a) Track plot.

(b) Fourier series fit.
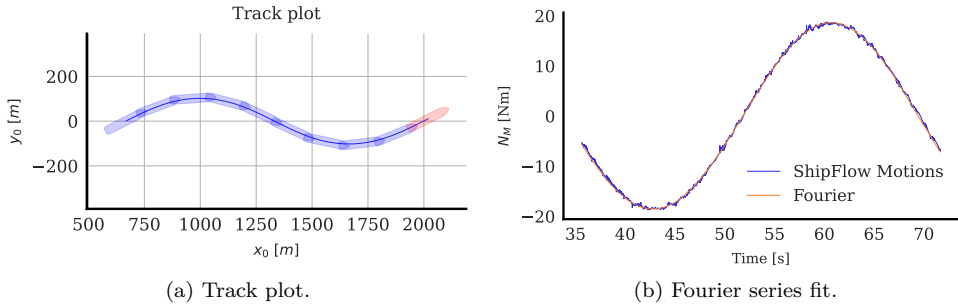
Figure 3.2: Pure yaw ShipFlow Motions results to determine the yaw added mass.

3.3   Roll model parameter estimation

Damping parameters can be estimated directly from the VCT forces, as demonstrated in section 3.1. However, this approach is infeasible when the ship is free to move, necessitating the use of FT time series data to estimate the parameters. In such cases, the full dynamics must be considered. The damping parameters (B_1, B_2, B_3) and stiffness parameters (C_1, C_3, C_5) can be identified from the parametric linear, quadratic, and cubic roll motion model structures presented in the previous chapter (Eq. (2.4), Eq. (2.5), and Eq. (2.6)). These equations do not have unique solutions because each equation can be multiplied by an arbitrary factor to yield a new valid solution. Unique solutions can be obtained through excluding inertia by normalizing the equations with the total roll inertia A_{44}, as shown in Eq. (3.14) for the linear model.

$$\ddot{\phi} + \frac{B_1}{A_{44}}\dot{\phi} + \frac{C_1}{A_{44}}\phi = \ddot{\phi} + B_{1A}\dot{\phi} + C_{1A}\phi = 0 \tag{3.14}$$

The identified normalized damping and stiffness parameters, B_{1A} and C_{1A}, can be expressed in dimensional units by multiplication with the normalization factor A_{44}.

If A_{44} is unknown beforehand, it can be calculated using Eq. (3.15) (Piehl 2016), assuming that the metacenter height, GM, is known.

$$A_{44} = \frac{GMgm}{\omega_0^2} \tag{3.15}$$

The frequency, ω_0, can be obtained with a fast Fourier transform (FFT) of the roll signal. Two methods for parameter estimation have been investigated: the "derivation approach", referred to in IMO (2006), and the "integration approach", used in Söder et al. (2019), which are both described in the following subsections.

In inverse dynamics regression (referred to as the derivation approach in Paper 1), Eq. (3.14) is treated as a linear regression problem, where the states (ϕ, $\dot{\phi}$, and $\ddot{\phi}$) are known and the parameters B_1 and C_1 must be regressed. Only the roll angle ϕ is known from the experimental data, which means that the velocity and acceleration $\dot{\phi}$, $\ddot{\phi}$ must also be approximated (note that this is accomplished through numerical differentiation in Paper 1 and with the extended Kalman filter (EKF) in Paper 3). A least-squares fit is applied to the roll motion equation to identify the damping and stiffness parameters.

In the integration approach, Eq. (3.14) is solved as an ordinary differential equation (ODE) for many estimated sets of parameters until the solution converges. This method is time-consuming, and convergence is not guaranteed. However, the advantage is that only the roll angle ϕ is needed.

3.4   Inverse dynamics

Inverse dynamics (ID) was found to be an efficient method for identifying the parameters within the roll motion models. ID is a widely used technique in robotics (Faber et al. 2018; Haninger and Tomizuka 2019; Mastalli et al. 2023; Sun and Ding 2023; Kurtz et al. 2023) that is also highly applicable to ship dynamics. It can be used to estimate the total forces that act on a ship during motion. The technique can be applied to data from free-model manoeuvring tests or real ship maneuvers. The forces acting on a ship during a maneuver can be estimated using inverse dynamics applied to the equation of motion (Eq. (2.10)) when the mass matrix $\mathbf{M}$ and the acceleration vector $\dot{\boldsymbol{v}}$ are known. The hydrodynamic damping forces can be calculated by inserting the total force $\mathbf{F}$ from Eq. (2.16) into Eq. (2.10) and then solving for X_D, Y_D, and N_D, as shown in:

$$
\begin{aligned}
X_D &= -X_{\dot{u}}\dot{u} + Y_{\dot{r}}r^2 + Y_{\dot{v}}rv + \dot{u}m - mr^2 x_G - mrv \\
Y_D &= -X_{\dot{u}}ru - Y_{\dot{r}}\dot{r} - Y_{\dot{v}}\dot{v} + \dot{r}mx_G + \dot{v}m + mru \\
N_D &= I_z\dot{r} - N_{\dot{r}}\dot{r} - N_{\dot{v}}\dot{v} + X_{\dot{u}}uv - Y_{\dot{r}}ru - Y_{\dot{v}}uv + \dot{v}mx_G + mrux_G
\end{aligned}
\tag{3.16}
$$

These expressions are used to estimate the forces acting on a ship during FRMTs, for example, as shown for a turning circle test in Figure 3.3. The estimated inverse dynamics forces were used in Paper 3 and 4 as inputs for an inverse dynamics regression (see section 3.6). An inverse dynamics approach was also used in Paper 4 and 5 to

estimate the forces acting on the ship during the FRMTs, which were then compared with the model force predictions. This is a more informative approach to assessing model performance than, for instance, using open-loop or closed-loop simulations. The benefit is that the model and the experiment will always be in the same state, which is not the case when simulations are used.

(a) Track plot.
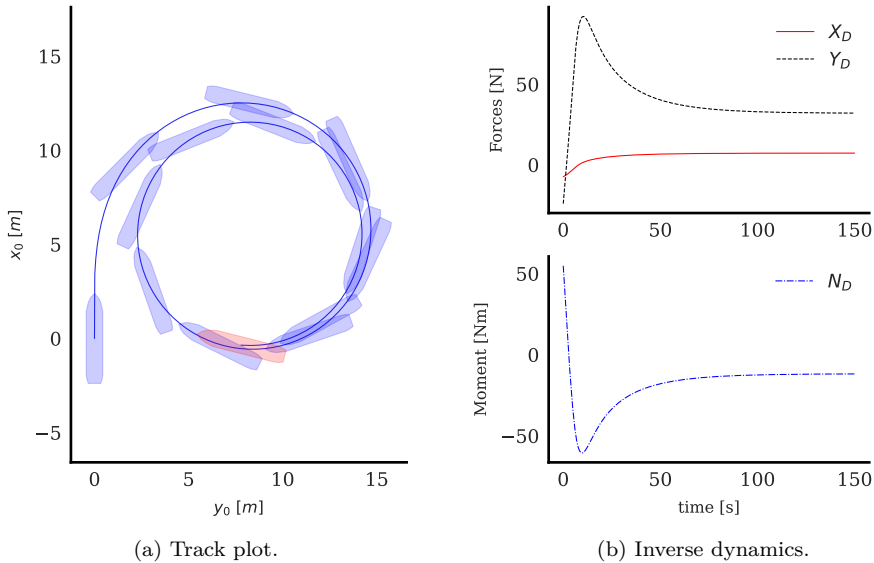
(b) Inverse dynamics.

Figure 3.3: Forces and moments calculated with inverse dynamics on data from a turning circle test.

3.5   Data cleaning

It is possible to perform an exact parameter estimation on flawless (simulated) data with no noise (see Paper 3). However, such ideal data from physical experiments do not exist in reality. Measured data will always contain both process noise and measurement noise. Even very moderate measurement noise can create significant problems for inverse dynamics in cases where noise is amplified when velocities and accelerations are differentiated from measured positions. Mitigation of the effects of noise can be achieved if the data are pre-processed using the extended Kalman filter (EKF) (Brown and Hwang 1997) and the Rauch-Tung-Striebel (RTS) smoother (Rauch et al. 1965), both of which are presented below.

EKF is an extension of the Kalman filter (KF) that is used for nonlinear systems, such as manoeuvring models. The premise is that noise can be neglected in the absence of a plausible physical explanation. For instance, if noisy measurement data were entirely correct, it would imply that large ship vibrations resulted from large high-frequency forces (given the size of the ship). A prior understanding of the system dynamics suggests that these forces are not present. Therefore, the noise

should be considered measurement noise and should be removed. Low-pass filtering is commonly used to remove noise, where motions above a cutoff frequency are considered unphysical measurement noise. However, choosing this cutoff frequency is difficult. It is often either too low (removing some of the signal) or too high (retaining some unfiltered measurement noise in the data). The Kalman filter has a predictor model, a manoeuvring model in this case, that continuously estimates the system's state that runs parallel with the measurement data. The filter estimates the current state as a combination of the measurement data and the predictor model estimate based on the possible validity of the data and the model. If the data has low noise, the estimate is closer to that data. Conversely, if the model provides very accurate predictions, then that estimate is closer to the model. The system's inverse dynamics require everything about the state (positions, velocities, and accelerations) to be known. Only positions are known from the measurements, so the velocities and accelerations are instead estimated by the EKF.

The EKF is recursive and updates estimates in real-time as new measurements become available. It uses past measurements to predict states in the near future, making it useful for online applications, such as autopilots or autonomous ships. However, this real-time constraint is unnecessary for the estimation of pre-existing data, where an entire time series of existing measurements is available. In such cases, knowledge of both past and future data can be used to improve the filter. Future time steps can be included by applying the RTS smoother after the filter. The RTS smoother algorithm runs the EKF in reverse to account for future time steps. The EKF recursive algorithm used is summarized in the pseudo-code in Figure 3.4 (Brown and Hwang 1997).

Algorithm 3.1 (Discrete-time extended Kalman filter)
Inputs
   Initial values: $\mathbf{x_0}$, $\mathbf{P_0}$
   Filter parameters: $\mathbf{C_d}$, $\mathbf{R_d}$, $\mathbf{Q_d}$, $\mathbf{E_d}$
   Data: $\mathbf{y}$, $\mathbf{c}$
Output
   Estimated states: $\hat{\mathbf{x}}$, estimated state covariances $\hat{\mathbf{P}}$

1. Initial values:
   1. $\hat{\mathbf{x}}[0] = \mathbf{x_0}$
   2. $\hat{\mathbf{P}}[0] = \mathbf{P_0}$
2. For k in n measurements (time steps)
   1. KF gain
      1. $\mathbf{K}[k] = \hat{\mathbf{P}}[k]\mathbf{C_d}^T \left(\mathbf{C_d}\hat{\mathbf{P}}[k]\mathbf{C_d}^T + \mathbf{R_d}\right)^{-1}$
      2. $\mathbf{I_{KC}} = \mathbf{I_n} - \mathbf{K}[k]\mathbf{C_d}$
   2. Update
      1. State corrector $\hat{\mathbf{x}}[k] = \hat{\mathbf{x}}[k] + \mathbf{K}[k](\mathbf{y} - \mathbf{C_d}\hat{\mathbf{x}}[k])$
      2. Covariance corrector $\hat{\mathbf{P}}[k] = \mathbf{I_{KC}} \cdot \hat{\mathbf{P}}[k]\mathbf{I_{KC}}^T + \mathbf{K}[k]\mathbf{R_d}\mathbf{K}^T$
   3. Predict
      1. State predictor $\hat{\mathbf{x}}[k+1] = \hat{\mathbf{x}}[k] + h \cdot \hat{\mathbf{f}}(\hat{\mathbf{x}}[k], \mathbf{c}[k])$
      2. Covariance predictor $\hat{\mathbf{P}}[k+1] = \mathbf{A_d}[k]\hat{\mathbf{P}}[k]\mathbf{A_d}[k]^T + \mathbf{E_d}\mathbf{Q_d}\mathbf{E_d}^T$

Figure 3.4: Algorithm for a discrete time extended Kalman filter.

Here, n is the number of states (6 in this case), and $\mathbf{I_n}$ is an n by n identity matrix. The transition matrix is calculated for each iteration using the Jacobian of the transition model:

$$\mathbf{A_d}[k] = \mathbf{I_n} + h \left.\frac{\partial f\left(\mathbf{x}[k], \mathbf{c}[k]\right)}{\partial \mathbf{x}[k]}\right|_{\mathbf{x}[k] = \hat{\mathbf{x}}[k]} \tag{3.17}$$

This formulation and the fact that the nonlinear transition model is used directly as the predictor are the key differences between the EKF and the linear KF. Please note the linear approximation in Eq. (3.17) around the current state. This approximation can cause instability if the real system and the linearized system deviate significantly when large time steps are used on a very nonlinear system. The unscented Kalman filter, which was used in Revestido Herrero and Velasco González (2012), is an alternative that can be applied in such situations.

   The output from the filter contains the estimated states: $\hat{\mathbf{x}}$ and the estimated state covariance matrix $\hat{\mathbf{P}}$. $\hat{\mathbf{x}}$ represents the most likely estimates, but these estimates have uncertainty that is expressed in $\hat{\mathbf{P}}$. The state of the system is described by the ship's position, heading, velocities, and yaw velocity:

$$\mathbf{x} = [x_0, y_0, \psi, u, v, r]^T \tag{3.18}$$

The initial state x_0 is taken as the mean value of the first five measurements, where the velocities are estimated using numeric differentiation. $\mathbf{C_d}$ selects the measured states (x_0, y_0, ψ):

$$\mathbf{C_d} = h \begin{bmatrix} 1 & 0 & 0 & 0 & 0 & 0 \\ 0 & 1 & 0 & 0 & 0 & 0 \\ 0 & 0 & 1 & 0 & 0 & 0 \end{bmatrix} \tag{3.19}$$

$\mathbf{E_d}$ selects the hidden states (u, v, r):

$$\mathbf{E_d} = h \begin{bmatrix} 0 & 0 & 0 \\ 0 & 0 & 0 \\ 0 & 0 & 0 \\ 1 & 0 & 0 \\ 0 & 1 & 0 \\ 0 & 0 & 1 \end{bmatrix} \tag{3.20}$$

where h is the discrete time step, $\mathbf{R_d}$ describes the covariance matrix of the measurement, $\mathbf{Q_d}$ is the covariance matrix of the process model, and $\mathbf{P_0}$ is the initial state covariance. Selecting appropriate values for these three matrices is the most challenging aspect of optimizing EKF performance. The matrix $\mathbf{R_d}$ should reflect the expected measurement noise, and $\mathbf{Q_d}$ should account for the uncertainty introduced by the process model (manoeuvring model) .

3.6   Parameter estimation from inverse dynamics

Parameter estimation from CT data (CMT or VCT), as described in section 3.1, is the classic approach to identifying parameters within a manoeuvring model. However, a model can also be identified from time series FT data obtained with FRMTs or full-scale maneuvers. Rather than, as in the CMT or VCT, directly measuring forces, they can be estimated through the application of inverse dynamics (see section 3.4). However, inverse dynamics is inherently limited in estimating rudder forces, which affects the estimation accuracy of the other manoeuvring coefficients (Araki et al. 2012). It may be difficult to determine where the forces are generated by solely considering the total force, which introduces a high multicollinearity between the hull and the rudder forces during the maneuvers. This can be addressed by measuring the rudder force, as demonstrated in the Optiwise test case in Paper 5. Otherwise, the rudder force must be estimated, which was investigated in Paper 4 by introducing a semi-empirical rudder model (see subsection 2.5.1). The hull forces needed to regress the hull coefficients can be estimated by subtracting the rudder and propeller forces from the total damping forces according to Eq. (3.4)–Eq. (3.6).

3.7 Recursive inverse dynamics regression

A new parameter estimation method is proposed in Paper 3 for the manoeuvring model structures. This approach involves solving the reversed manoeuvring problem, where unknown forces are predicted from known manoeuvring model test data. The hydrodynamic derivatives in the manoeuvring model are estimated by performing regression, where force polynomials are used to approximate the forces predicted with inverse dynamics. (see section 3.4). Measurement noise must be removed prior to the regression of hydrodynamic derivatives in the manoeuvring model. This is implemented through an extended Kalman filter (EKF) and a Rauch Tung Striebel (RTS) smoother (see section 3.5). The EKF requires an accurate manoeuvring model as the predictor. Therefore, the accurate manoeuvring model is both the input and output of the method. As a solution to this dilemma, the initial predictor is a linear manoeuvring model that includes hydrodynamic derivatives estimated with semi-empirical formulas taken from Brix (1993), as described in Paper 3. Once the regressed manoeuvring model has been obtained, the parameter estimation can be refined, using the regressed manoeuvring model as the predictor model in the EKF, thereby improving the filter and obtaining a more accurate manoeuvring model. This method is summarized in Figure 3.5 and can be repeated several times (as indicated by the dashed arrow) for improved accuracy.
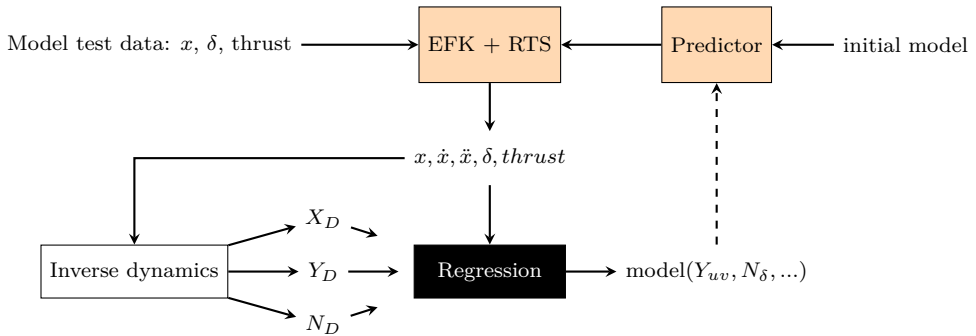
Figure 3.5: Method to estimate the manoeuvring model hydrodynamic derivatives.

Using semi-empirical formulas for the initially estimated manoeuvring model adds prior knowledge of the ship dynamics to the regression. An example, with simulation results from the steps in the iteration, is presented in Figure 3.6.
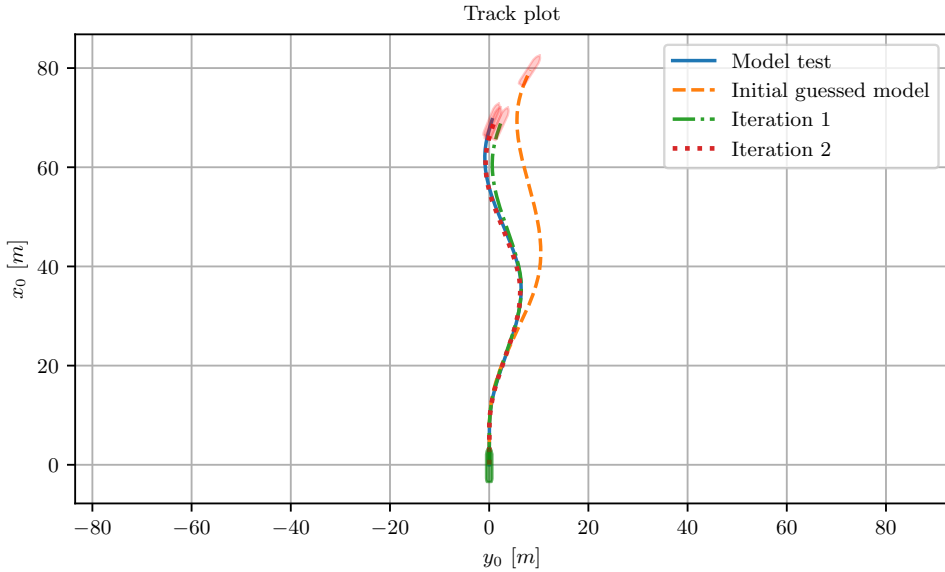
Figure 3.6: Simulation with: initial model and first and second iteration of the parameter estimation method.

3.8 Test cases

Two test cases have been studied in this thesis. The wPCC test case is a ship that was designed for a wind-assisted propulsion system (WAPS) and is capable of operating in a fully sailing mode, a fully motoring mode, and intermediate states. However, this thesis only considers the motoring mode. The wPCC design differs slightly from conventional motoring cargo ship designs because of the WAPS. It has two very large rudders, which are two to three times larger than those needed for a conventional ship. The ship also has fins at the bilge to generate extra lift while sailing, as shown on the scale model in Figure 3.7. Table 3.3 shows the main particulars of the scale model.

Figure 3.7: Scale model of the wPCC used in the model tests. Copyright RISE.

The Optiwse test case is based on a typical VLCC tanker but features a larger rudder size adapted for the WAPS, as shown in the scale model in Figure 3.8. Table 3.3 shows the main particulars of the scale model.
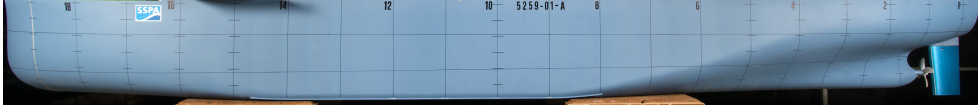
Figure 3.8: Scale model of the Optiwise used in the model tests. Copyright RISE.

Table 3.3: Main particulars of the test case scale models.

Parameter		wPCC	Optiwise	Description
A_R	m2	$3.01 \cdot 10^{-2}$	$3.48 \cdot 10^{-2}$	Projected rudder area
B	m	0.95	0.88	Breadth
D	m	0.12	0.16	Propeller diameter
I_{zz}	kg m2	742.05	1,471.51	Yaw moment of inertia around L/2
L	m	5.01	4.78	Length between perpendiculars
T_m	m	0.21	0.3	Mean draught
b_R	m	0.17	0.22	Rudder height
c_r	m	0.19	0.17	Rudder root chord
c_t	m	0.15	0.15	Rudder tip chord
m	kg	441.03	1,008.73	Ship mass
Scale factor	-	41.2	68	
t_{df}	-	0.12	0.21	Thrust deduction factor
x_G	m	-0.24	0.18	Longitudinal c.o.g.
x_R	m	-2.45	-2.39	Rudder position from L/2

3.9   Datasets

The data used in this thesis have been summarized in Table 3.4, which specifies the papers in which they were used, the testing facilities from which they were collected, and their corresponding references. Data from the 250 roll decay tests at SSPA could not be published, due to IP rights. The wPCC dataset was published in two versions, A and B. wPCC A was used in Paper 3 where the motions were expressed in the center of gravity. wPCC B was used in Papers 4 and 5 were the motions were instead expressed at the origin, as defined in section 2.2.

Table 3.4: Datasets used in this thesis.

Dataset	Paper	Facility	Reference
250 roll decay tests	1	SSPA	Unpublished due to IP rights
Roll decay KVLCC2	2	SSPA	Alexandersson and Kjellberg (2021)
wPCC A	3	SSPA	Alexandersson (2022)
KVLCC2 HSVA	3	HSVA	SIMMAN2008 (Stern et al. 2011)
KVLCC2 MARIN	3	MARIN	SIMMAN2008 (Stern et al. 2011)
wPCC B	4 & 5	SSPA	Alexandersson (2024)
Optiwise	5	SSPA	Unpublished

Chapter 4

Summary of papers

This chapter presents a summary of the papers appended to this thesis, which includes research activities and a selection of the most relevant results. The relationships between the papers are summarized in Figure 4.1. The first two papers focus on the roll motion, in which the work conducted using Ikeda's method in Paper 1 is continued in Paper 2. The work exploring inverse dynamics that was initiated in the roll motion papers continued in the remaining manoeuvring papers. Multicollinearity was found to be a significant challenge in Paper 3, and was initially addressed through model truncation. However, model generalization may be reduced when model truncation is used, which was shown in Paper 4. Instead, the multicollinearity between the hull and rudder forces was mitigated by introducing a semi-empirical rudder model. The multicollinearity between the drift and yaw rate dependent forces was subsequently addressed in Paper 5. In addition, see Table 1.2 in section 1.3 for a discussion of the relationship between these papers and the research objectives of this thesis.
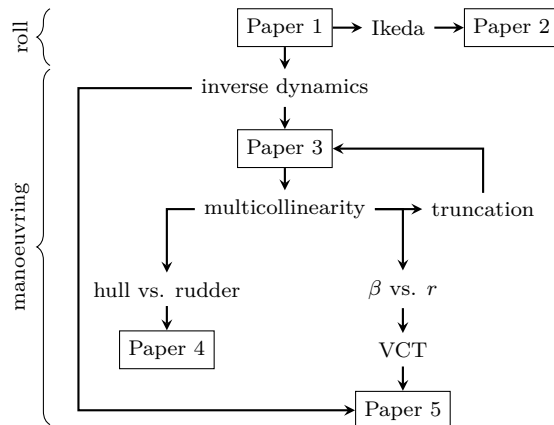
Figure 4.1: Paper connections.

4.1 Summary of Paper 1

"Analysis of roll damping model scale data"

Scope and motivations

The initial step in this research project was to simplify the system identification of ship dynamics to a single degree of freedom, specifically roll motion. However, this is still a very important subject where accurate modeling of roll motion is crucial, as France et al. (2001) demonstrated in their investigation of the APL China casualty in

1998. In this incident, a post-Panamax C11 class container ship lost nearly a third of its containers, most likely due to head sea parametric rolling.

Results and main findings

The objective of Paper 1 was to develop parameter identification techniques for roll motion models derived from roll decay model tests. Additionally, it aimed to propose a parametric model structure for roll motion dynamics that generalizes well, based on prior knowledge from these model tests.

Roll damping was studied using time series data from 250 roll decay tests executed by RISE at the SSPA Maritime Center Maritime Dynamics Laboratory. System identification was conducted on each of these time series using linear, quadratic, and cubic models. Simulation results from the identified models for one of the 250 roll-decay tests is compared to the corresponding experimental results in Figure 4.2. The cubic and quadratic models satisfactorily reproduced the results of this roll decay test, but the linear model was too simplified an approach to provide an accurate representation for both smaller and larger roll angles.

A more detailed analysis can be achieved through consderation of the amplitude decrement ϕ_a and roll damping B for each oscillation as shown in Figure 4.3. Figure 4.3b shows that none of the models perfectly fit the damping in this particular example, which seems to be caused by difficulties in determining the damping for smaller amplitudes, where a high scatter can be observed. However, a more rational approach to assessing the goodness of fit was adopted for all 250 roll decay tests, where the coefficient of determination R^2 was calculated for each fit as:

$$R^2 = 1 - \frac{SS_{res}}{SS_{tot}} R^2 = 1 - \frac{\sum_{i=1}^{n}(\phi_i - \hat{\phi}i)^2}{\sum_{i=1}^{n}(\phi_i - \bar{\phi})^2} \tag{4.1}$$

where ϕ_i is the model test roll angle at time step i, $\bar{\phi}$ is the mean roll angle from the model test, and $\hat{\phi}_i$ is the predicted roll angle (for the linear, quadratic, or cubic model). The average R^2 of all tests was calculated for each model, giving 0.995 for the cubic model, 0.993 for the quadratic model, and 0.986 for the linear model. These values indicate that the quadratic model is almost as accurate as the cubic model for describing roll motion. The quadratic model, with fewer parameters than the cubic model, is expected to have a higher level of generalization at the same accuracy and is therefore proposed as the best mathematical model for roll motion.
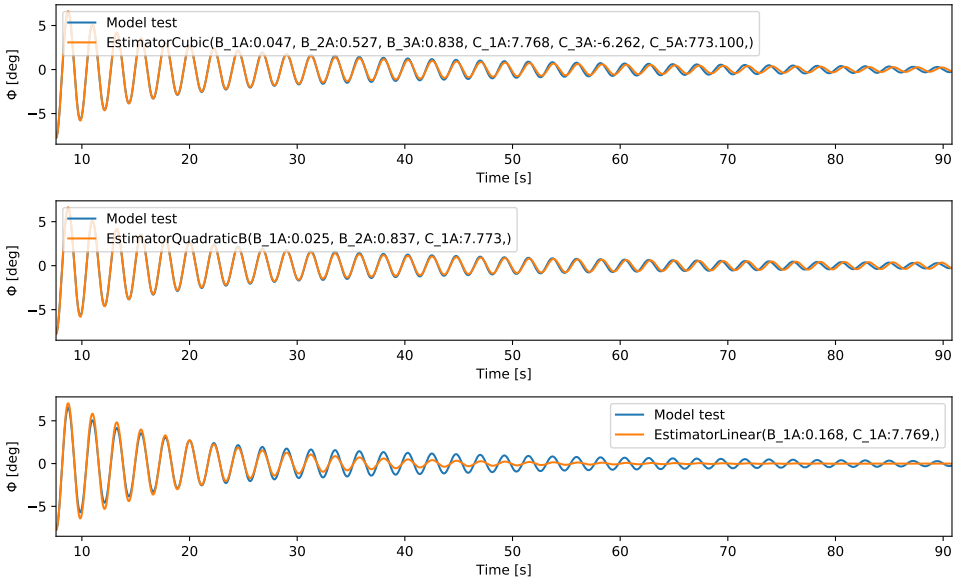
Figure 4.2: Roll decay estimation with identified cubic, quadratic, and linear models.
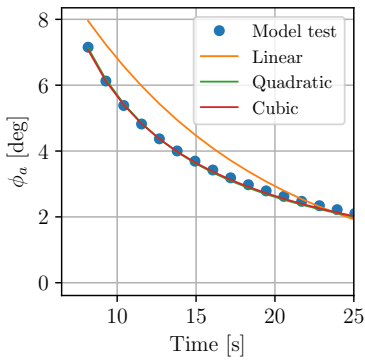
(a) Amplitude decrements.
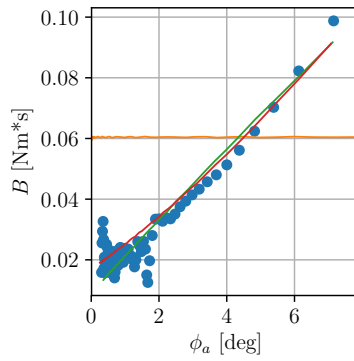
(b) Dampings.

Figure 4.3: Roll decay model test, linear-, quadratic-, and cubic-model.

4.2   Summary of Paper 2

"Prediction of roll motion using fully nonlinear potential flow and Ikeda's method"

Scope and motivations

An explicit semi-empirical formula was proposed in Paper 1, based on a simplified version of Ikeda's method (Kawahara et al. 2011). This is a very low computational cost alternative. However, it was also found to have poor accuracy, especially for modern ship designs. Paper 2 proposed a new hybrid method to address the shortcoming, where the viscous roll damping from Ikeda's semi-empirical method was injected into an existing 3D unsteady fully nonlinear potential flow (FNPF) method (Kjellberg 2013).

Results and main findings

Viscous roll damping was calculated using Ikeda's method (Ikeda et al. 1978) for the KVLCC2 test case. An error was encountered in the calculation of the C_r coefficient used to obtain the eddy damping at zero speed. The source of this error was traced to a regression formula from experiments conducted by Ikeda (1978) on several two-dimensional cylinders with various sections. A new regression was instead proposed, using a decision tree model. Fig.4.4 shows C_r from the experiments and corresponding predictions with Ikeda's method and the decision tree. The capital letters refer to cylinder sections from the experiments (Ikeda 1978).
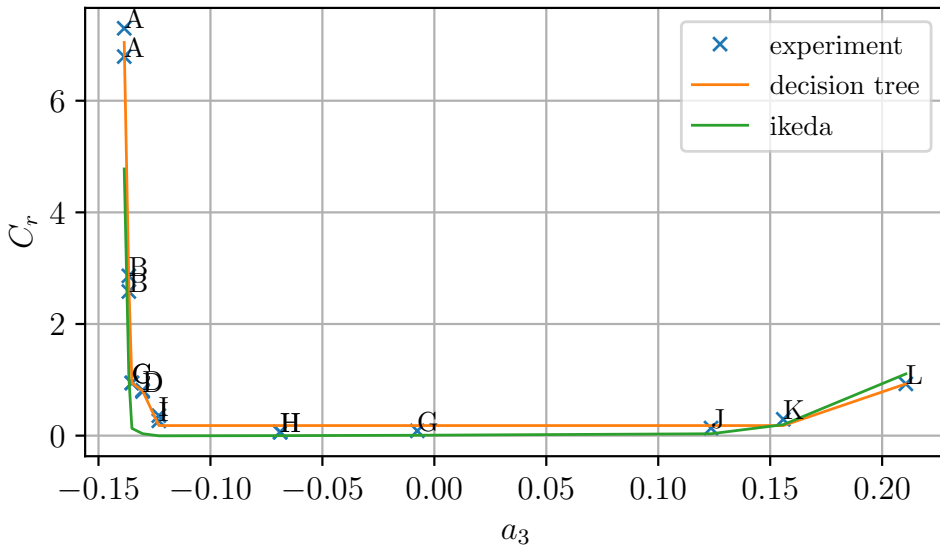
Figure 4.4: C_r for cylinder sections from experiments and predicted with Ikeda's method and the decision tree model.

The total predicted roll damping agreed satisfactorily with the damping of the model tests at zero speed (Figure 4.5) and showed excellent agreement at speed (Figure 4.6). Roll decay simulations with damping from the hybrid method were conducted. Results from these simulations were compared with the model tests at zero speed (Figure 4.7) and at speed (Figure 4.8). The time series from the corresponding FNPF simulations have also been added to these plots to demonstrate the influence of the injection of semi-empirical viscous damping on the accuracy of these simulations.

Paper 2 concluded that Ikeda's method offers an effective semi-empirical approach for predicting viscous roll damping. When combined with modern potential flow codes, such as FNPF, it enables highly accurate predictions of ship roll motion.
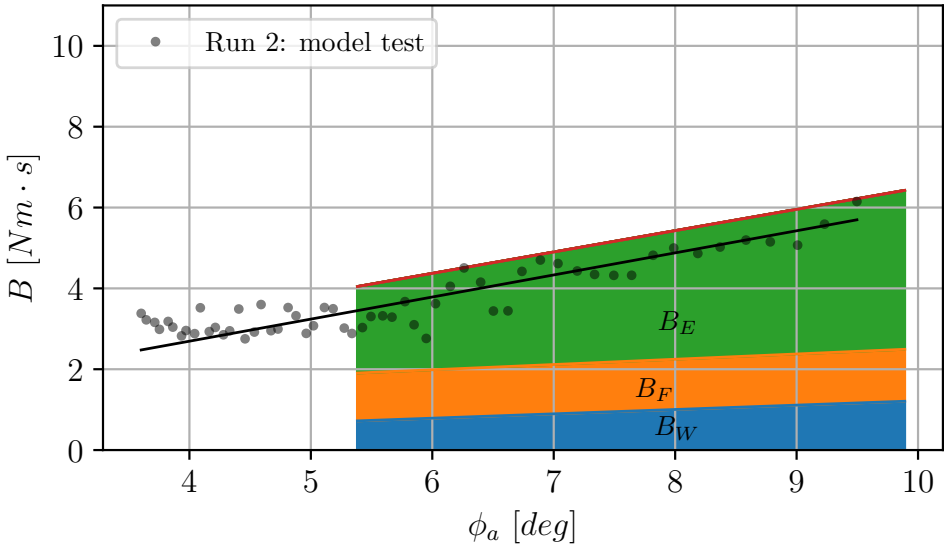
Figure 4.5: Roll damping from hybrid method ($F_n = 0$) for KVLCC2.
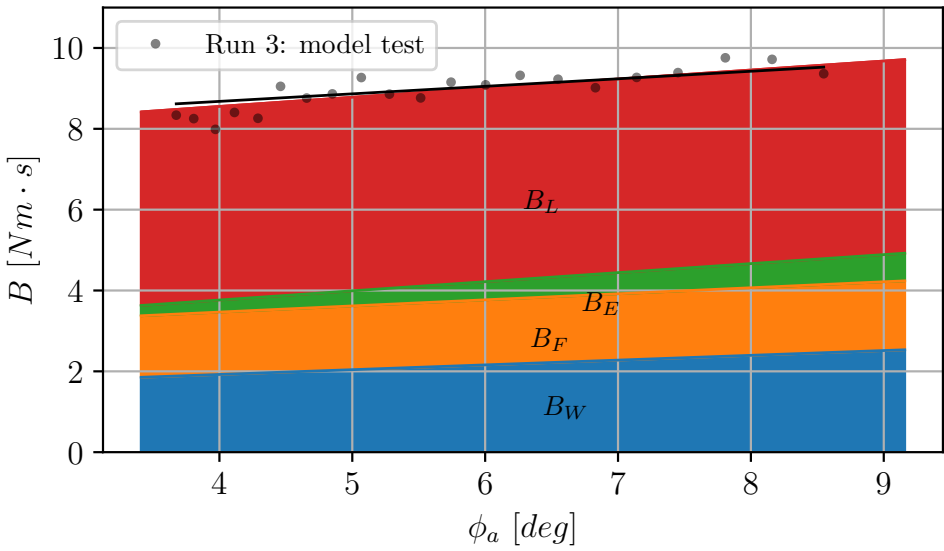
Figure 4.6: Roll damping from hybrid method ($F_n = 0.14$) for KVLCC2.
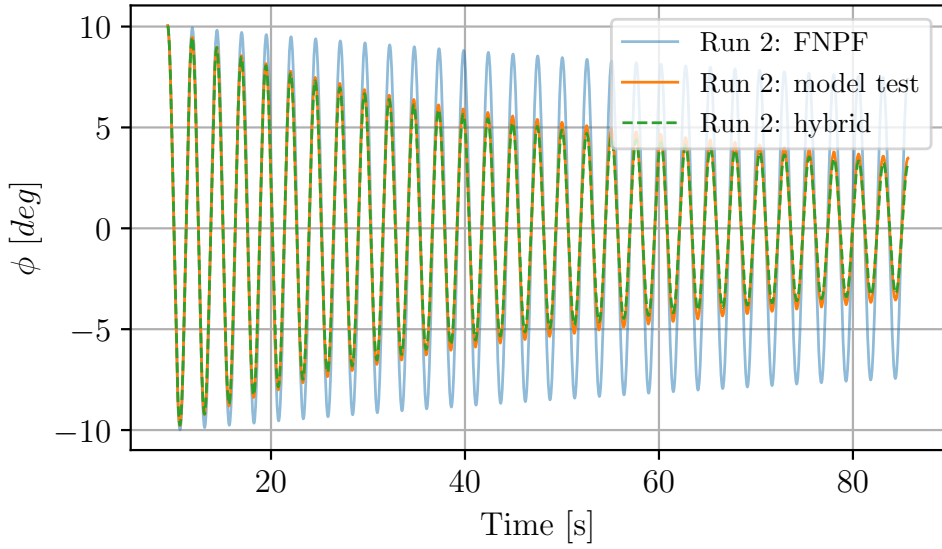
Figure 4.7: Roll decay ($F_n = 0$) for KVLCC2.
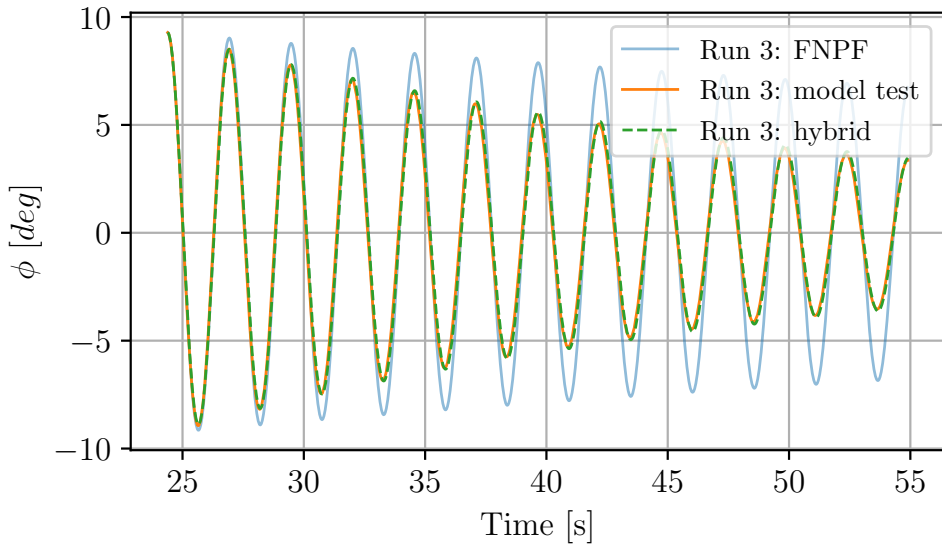
Figure 4.8: Roll decay ($F_n = 0.14$) for KVLCC2.

4.3   Summary of Paper 3

"System identification of vessel manoeuvring models"

Scope and motivations

The modeling complexity and uncertainty from Paper 1 were addressed in Paper 3, in which system identification of manoeuvring through the addition of surge, sway, and yaw degrees of freedom was studied. The objectives were to find parametric model structures with good generalization and to develop parameter identification techniques from FT data.

The dynamics were assumed to be described by an Abkowitz or truncated Abkowitz model. The system identification method proposed in Paper 3 was validated using two case study ships: the wPCC and the KVLCC2 (Figure 4.9). The parameters were estimated through recursive inverse dynamics regression (see section 3.7). Identification was performed via cross validation using a hold-out evaluation approach (Sammut and Webb 2017). The data in this evaluation were divided into three sets: the training set, the validation set and the test set, as seen in Figure 4.10. The training set was used to fit all the candidate models using the proposed parameter estimation method, while the validation set was used to select the most effective model. The training and validation sets were subsequently combined to train the selected model, producing the final model, which was evaluated using the test set. Rather than being randomly partitioned, these three sets were structured to assess the model's extrapolation ability. The data sets were split such that the smallest yaw rates, drift-angles, and rudder-angles formed the training set, the validation set contained the medium values, and the largest values formed the test set. Examples of this can be seen for the two test cases in Figure 4.11 and Figure 4.12.

+

Figure 4.9: Ship model used in HSVA and MARIN model tests. Copyright HSVA.
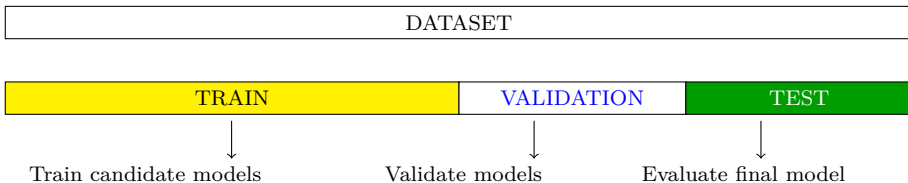
Figure 4.10: Model development process with hold-out evaluation.
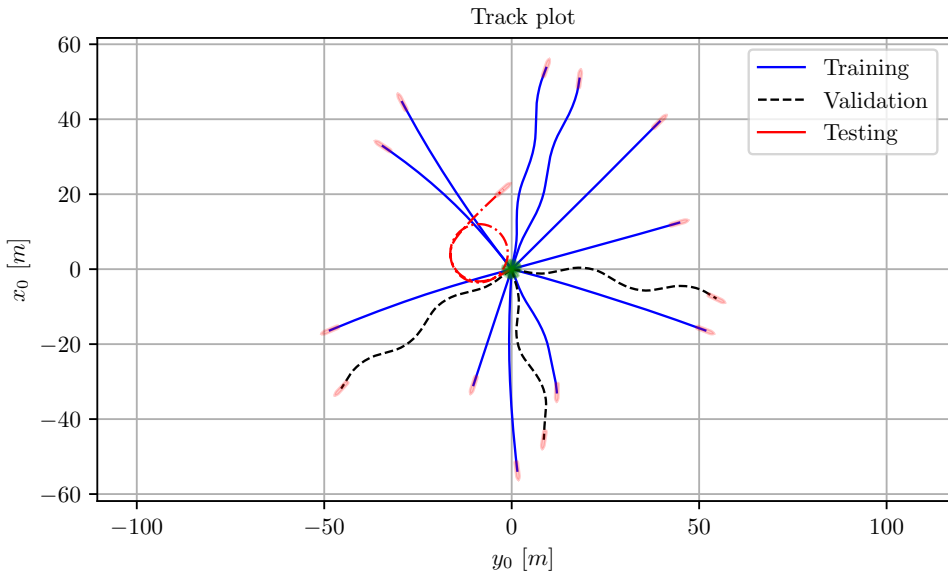
Figure 4.11: wPCC training, validation and testing datasets.
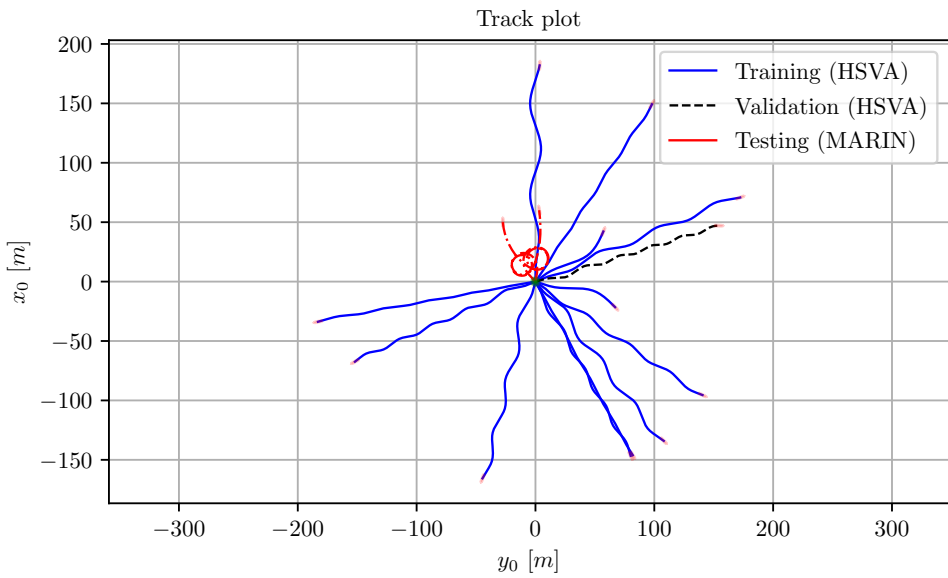
Figure 4.12: KVLCC2 training, validation and testing datasets.

Results and main findings

Figure 4.13 shows the predictions of the wPCC validation obtained using the identified models. AVMM is a full Abkowitz model and MAVMM is a truncated Abkowitz model where model structure selection has been applied. The AVMM model severely over-predicted the forces. This over-prediction was explained by the high multicollinearity of the AVMM model structure for the wPCC data, as shown in Figure 4.14 where the absolute correlation coefficient between the regressor variables in the wPCC yaw moment regression is presented. Very black cells indicate a high correlation between the two intersecting regressor variables. Therefore, simulations of the validation cases were only possible using the MAVMM. The MAVMM model was retrained on the combined test and validation data to obtain the final prediction model, which was used to predict the turning circle test data as shown in Figure 4.15. The advance and tactical diameter (IMO 2002) from the prediction differ by 4% and 1%, respectively. Monte Carlo simulations with alternative realizations of the regression, considering the uncertainty in the regressed parameters, are also displayed in these figures. The alternative realizations have similar simulation results to the model with mean values of the regression (black line).
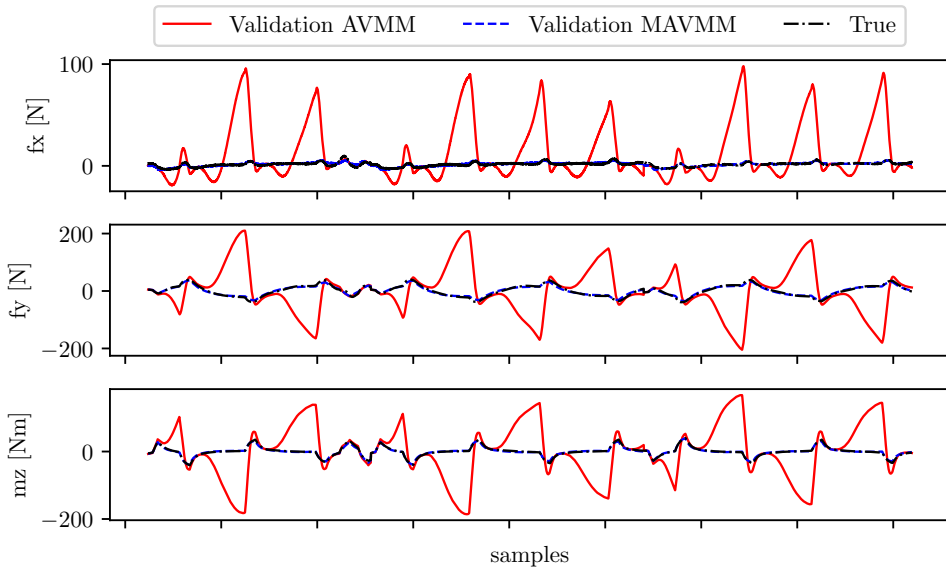
Figure 4.13: Validation of force models for wPCC ZigZag20/20.
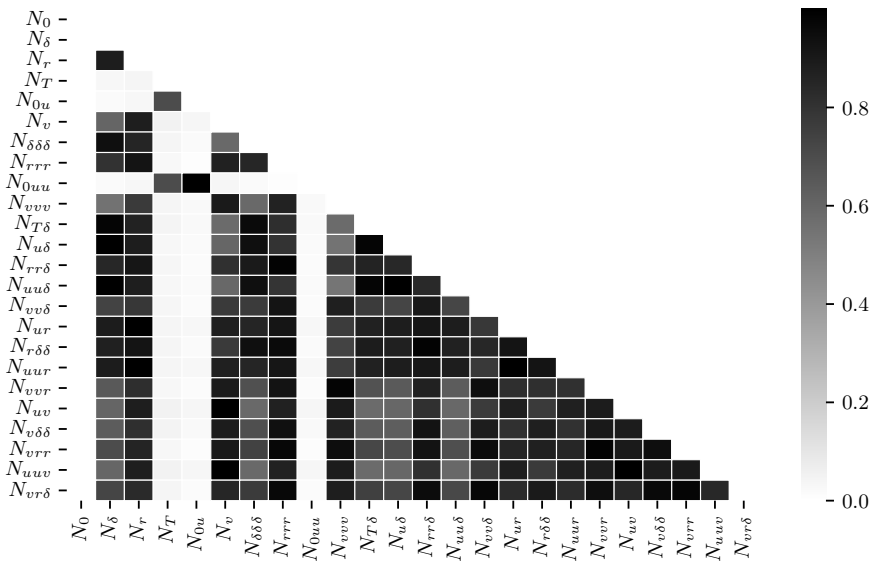
Figure 4.14: Absolute correlation between the regressor variables in the wPCC yaw moment regression of AVMM.
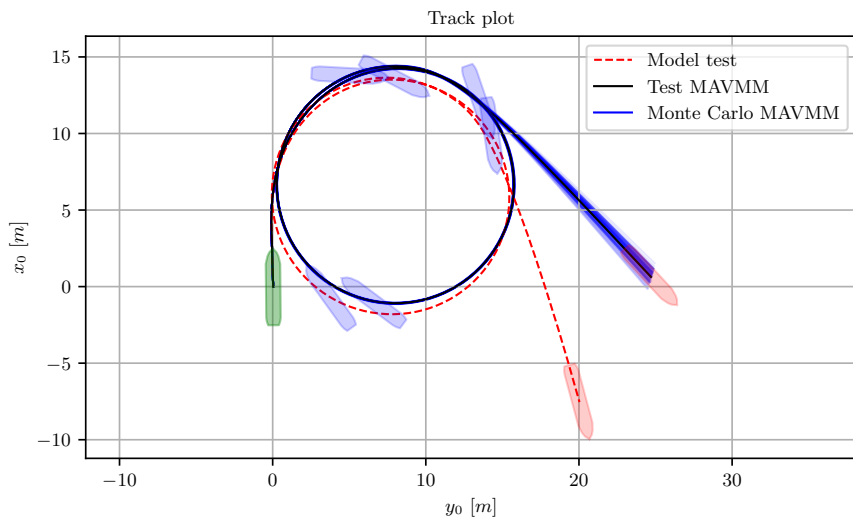
(a) Track plots.
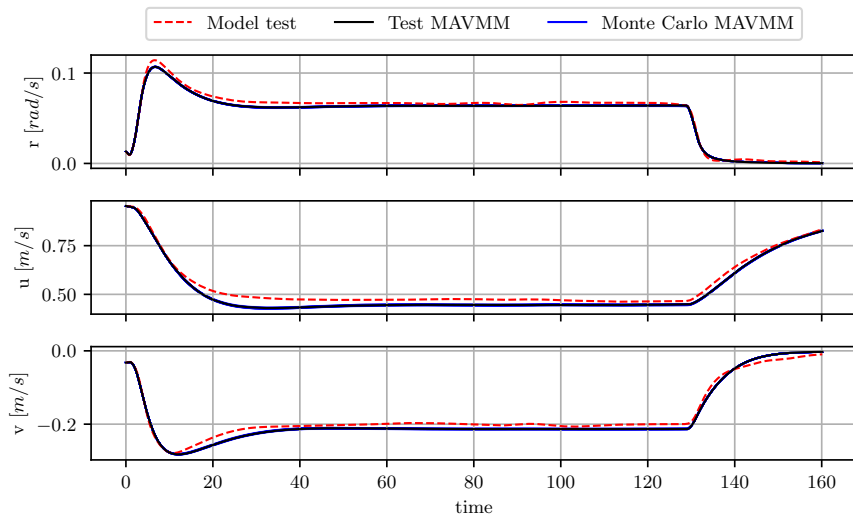
(b) Time series.

Figure 4.15: Turning circle test case for wPCC from model test and simulations.

The corresponding final prediction of the turning circle test for the KVLCC2 test case is shown in Figure 4.16. The prediction was conducted via simulation with the MAVMM trained on the training and validation data. Monte Carlo simulations with alternative realizations of the regression are also displayed in this figure. The alternative realizations are very similar to the simulation with mean values of the regression (black line). The predicted advance and tactical diameters differ by 2% and 5%, respectively.
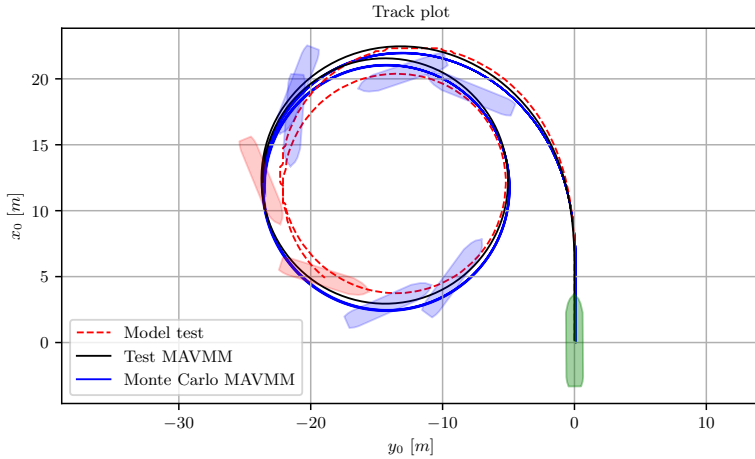
(a) Track plots.
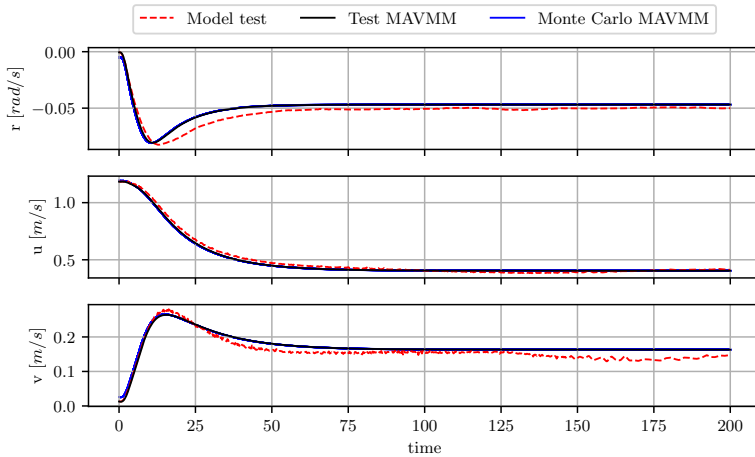
(b) Time series

Figure 4.16: Comparison between the predicted turning circle test with MAVMM trained on HSVA data and MARIN model test results for KVLCC2.

4.4   Summary of Paper 4

"System identification of a physics-informed ship model for better predictions in wind conditions"

Scope and motivations

Minimizing the number of regressor variables is often advisable to reduce the risk of overfitting to irrelevant data, aligning with the long-standing principle that "Nature is simple" (Ljung 2010). However, this prejudiced approach could also lead to model structures with limited applicability, as certain regression terms may only become significant under specific conditions, such as sailing in wind (Abkowitz 1980).

It was shown in Paper 3 that it is possible to identify a model from a calm water free running model test through inverse dynamics regression (section 3.6) together with a cross validation technique to find a truncated model that can predict other types of maneuvers with adequate accuracy. However, it was soon discovered that these models did not generalize well when wind forces were added to the simulations.

Paper 4 investigated this issue using two modular manoeuvring models. One of the models was a data-driven, physics-uninformed (PU) model, akin to the models used in the prior paper (Paper 3). The other model was a physics-informed (PI) model, which incorporated prior knowledge of rudder hydrodynamics to guide the identification toward a more physically correct model. The models had identical prediction models for the hull and propeller forces but different models for the rudder forces. The PI model had a deterministic semi-empirical rudder model, while the PU model had a data-driven mathematical rudder model. The ship manoeuvring models were similar to the MMG model (Yasukawa and Yoshimura 2015), apart from the difference in rudder models and some minor enhancements, such as the expression of the surge velocity as a perturbed velocity (see section 2.3), allowing for higher-order resistance coefficients.

A brief description of the workflow of Paper 4 is shown in Figure 4.17. The PI and PU models were identified from free-running model tests using inverse dynamics and regression. A reference model was established to assess physical correctness, where the PI model was instead identified based on VCT data. This reference model, based on CFD, was assumed to be an adequate representation of the ship's physics. Verification and comparisons between the models were carried out in the free-sailing model tests. The effect of incorporating a deterministic semi-empirical rudder model into the PI model on reducing multicollinearity and improving generalization was examined.

Reference model

System Identification

VCT

Free sailing
model tests

EKF

State & control variation

Forces/Moments

Y_D

Y_H

Y_R

Rudder angle δ

Inverse dynamics

Y_D

N_D

Time

Reference model

PI, PU models

Results

Parameter
drift

Physical
correctness

Generalization
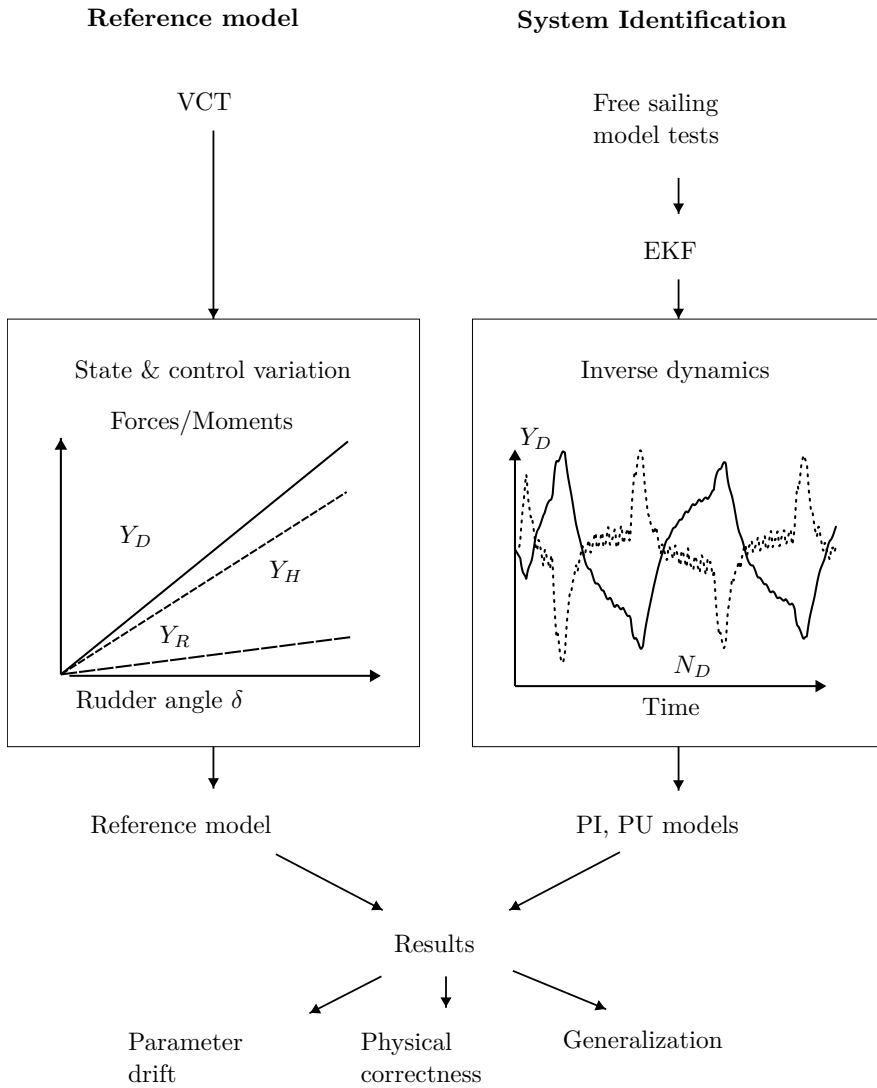
Figure 4.17: Research workflow, describing how the reference model is identified with regression of VCT data and the PI and PU models are identified with regression of inverse dynamics forces from model tests. Results are then gathered to assess the parameter drift, physical correctness and generalization of the models.

Results and main findings

Force predictions using reference, PI, and PU models for the states during one of the zigzag10/10 tests with wPCC were compared with the inverse dynamics forces for the same test in Figure 4.18. The PI and PU models predicted the same total yawing moment N_D and sway force Y_D as the reference model. However, the decomposition of this total yawing moment into components of the hull N_H and the rudder N_R differed significantly between the PU model and the PI and reference models, which were quite similar to each other.
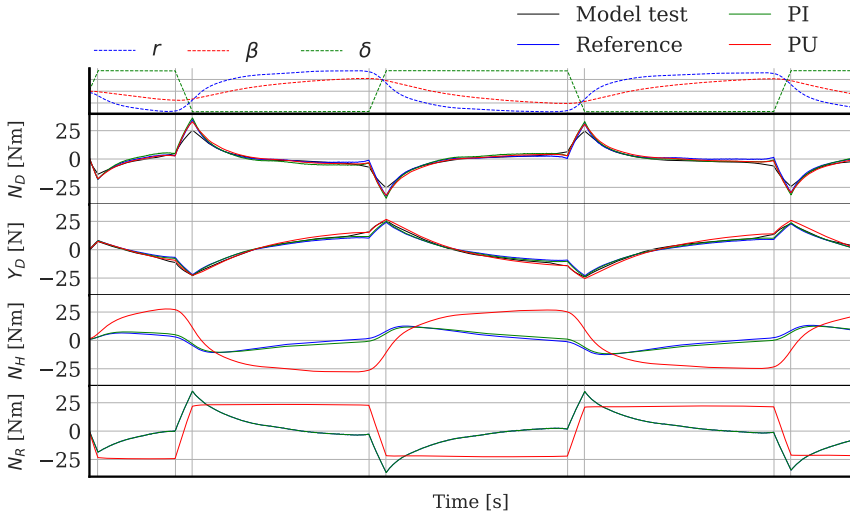
Figure 4.18: ID estimations of Y_D and N_D during a zigzag10/10 model test compared with model predictions.

The hull forces can be further decomposed into contributions from the drift of the vessel $N_H(v)$ and $Y_H(v)$, and contributions from the yaw rate $N_H(r)$ and $Y_H(r)$, as shown in Figure 4.19. It appears that almost all the yawing moments N_H depend on r for the PU model, and almost all the sway force Y_H is generated by v. This contrasts with the other two models, where both v and r contribute to N_H and Y_H.

Thus, the PU model not only misrepresents the decomposition between rudder and hull forces but also incorrectly separates the contributions of drift and yaw rate within the hull force model. However, this is not a significant problem during the zigzag tests, where the drift and yaw rate are highly correlated, as seen from the phase plot in Figure 4.20. This correlation can also explain why the completely data-driven model from the previous paper (Paper 3) performed well despite the erroneous decomposition.

However, when the ship is exposed to wind, causing changes in drift, the erroneous decomposition of the PU model becomes apparent, as shown in Figure 4.21. The PI model exhibits better alignment with the reference model under wind conditions.
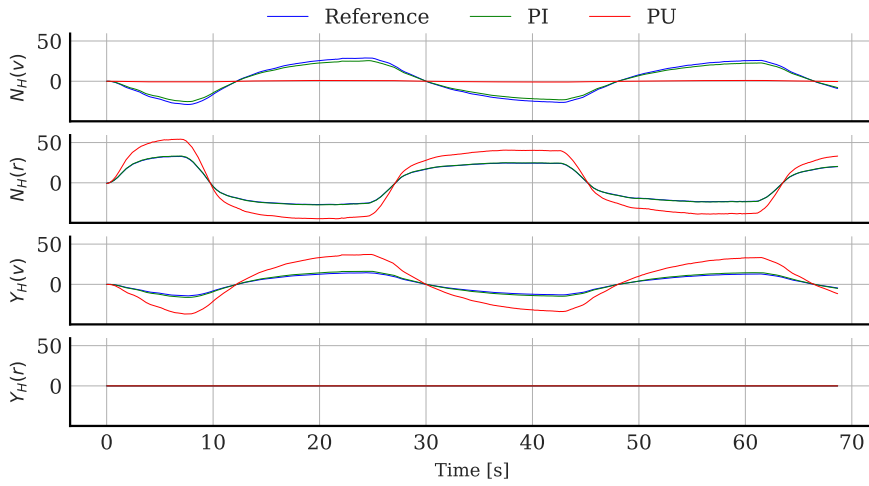
Figure 4.19: Decomposition of hull forces and moments during a zigzag20/20 test for parameters related to drift, yaw rate, and the prediction models.

Introducing a semi-empirical rudder model seems to have guided the identification toward a more physically accurate model, with lower multicollinearity and better generalization from calm water zigzag tests to wind conditions.
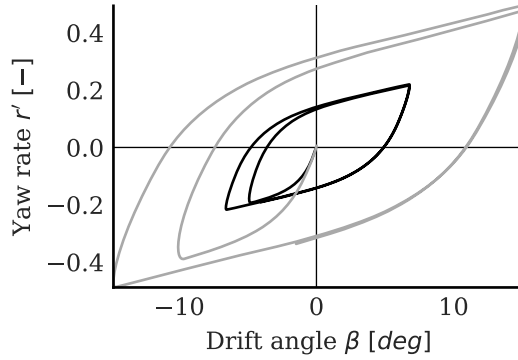
Figure 4.20: Phase portrait showing the combination of drift angle and yaw rate for zigzag10/10 and zigzag20/20 wPCC model tests.
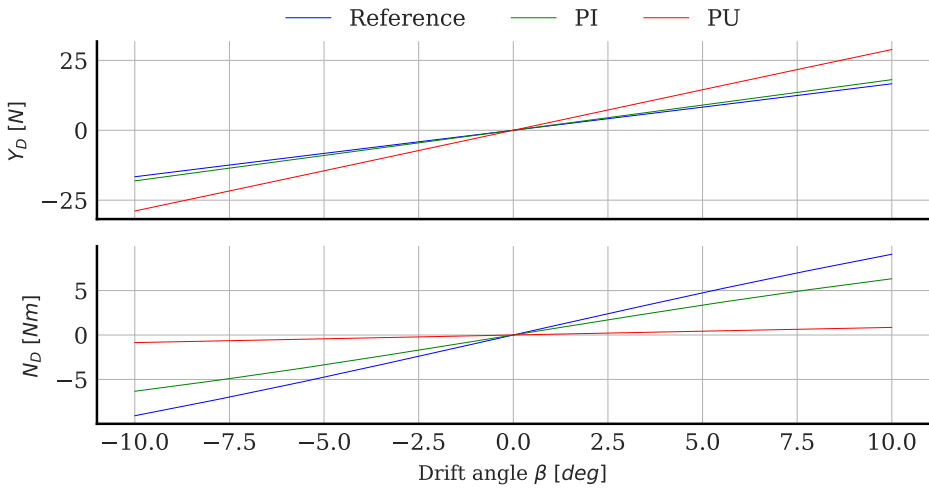
Figure 4.21: Total sway force and yawing moment from the wPCC models at various drift angles.

4.5   Summary of Paper 5

"Identification of manoeuvring models for wind-assisted ships with large rudders using virtual captive tests"

Scope and motivations

The objective of paper 5 was to propose a parametric model structure based on physical insights from VCT and FT inverse dynamics. The reference model from Paper 4 was assumed to be close to the physically correct true model of ship manoeuvring dynamics. This model was developed with VCT, which is based on physical first principles through CFD calculations. Paper 5 investigated the identification of manoeuvring with VCT more closely, with the aim of achieving a model that more accurately reflected the true system.

Manoeuvring models were developed for the two WAPS test cases with large rudders. The models were identified by conducting VCT to obtain hydrodynamic damping coefficients and by conducting pure yaw and pure sway tests in FNPF to obtain the added masses using the Fourier series method (see section 3.2). The identified force models were compared with the inverse dynamics forces of the zigzag tests to identify potential weaknesses within the models.

Results and main findings

Propeller and rudder forces were measured during the FRMTs for Optiwise. It was found that these measured forces together with forces predicted with a hull sub module, identified from VCT data, could recreate the estimated inverse dynamics forces during zigzag maneuvers with sufficient accuracy. Much effort was therefore devoted to finding a rudder force prediction model that could recreate the rudder forces for Optiwise. A modified quadratic MMG rudder model was proposed (see subsection 2.5.2) as an improved version of the original model (Yasukawa and Yoshimura 2015). Figure 4.22 shows the Optiwise rudder force Y_R for the various VCT test types (see section 3.1) plotted against the effective rudder angle β_R. The original MMG rudder model has a constant flow straightening factor γ_{Rpos} for positive β_R and another constant flow straightening factor γ_{Rneg} for negative β_R. The proposed quadratic formulation has two additional parameters, γ_{R2pos} and γ_{R2neg}, that allow the flow straightening to vary with β_R that better fits the VCT data.

The rudder forces during the Optiwise FRMTs were predicted and compared with the corresponding measured forces, as shown in Figure 4.23. Although there were some minor deviations during the zigzag10/10 test, there was generally good agreement between the predictions and measurements. VCT calculations of some of the states during the manoeuvres have also been added to this comparison, which also show good agreement.

The total forces during the zigzag tests were also predicted, including the hull and rudder models. Figure 4.24 shows a comparison between the predicted forces and FRMT inverse dynamics forces. VCT calculations of some of the states during the manoeuvres have also been added to this figure, which agrees well with the model

(a) Original MMG rudder model.

(b) Modified quadratic MMG rudder model.
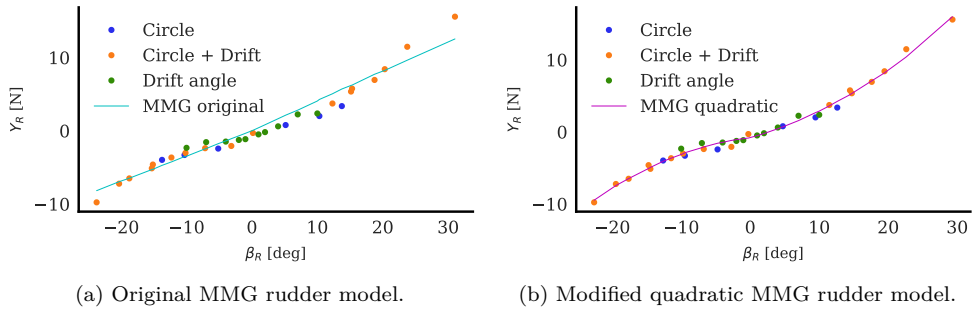
Figure 4.22: Rudder force during the VCT tests as a function of the effective inflow angle for the original MMG model and the modified quadratic MMG model.

(a) Zigzag10/10 to port.

(b) Zigzag20/20 to starboard.
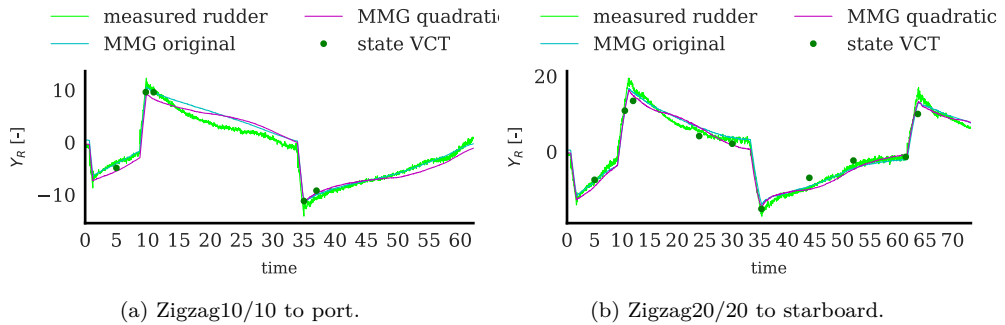
Figure 4.23: Rudder forces during the zigzag tests compared to predictions with the MMG models.

predictions. However, deviations were observed for the sway force Y_D within three seconds after the rudder changes at t = 11–14 s and t = 35–38 s, for the zigzag10/10 and t = 11–14 s, t = 35–38 s, t = 64 s, for the zigzag20/20. The model and state VCT calculations predict a straighter line in the Y_D time series near these deviation points. No reasonable explanation for these deviations has been found, and filtration errors in the EKF were ruled out as a possible explanation.

Closed loop simulations were also conducted, as shown in Figure 4.25, and exhibited strong agreement for the zigzag20/20 tests and a slightly lower agreement for the zigzag10/10 tests. It can therefore be concluded for the Optiwise case that the VCT data contained correct damping forces during the maneuvers, which were well described by the chosen model structure, including the proposed rudder model, and that the method used to determine added masses produced reasonable values.

(a) Zigzag10/10 to port.

(b) Zigzag20/20 to starboard.
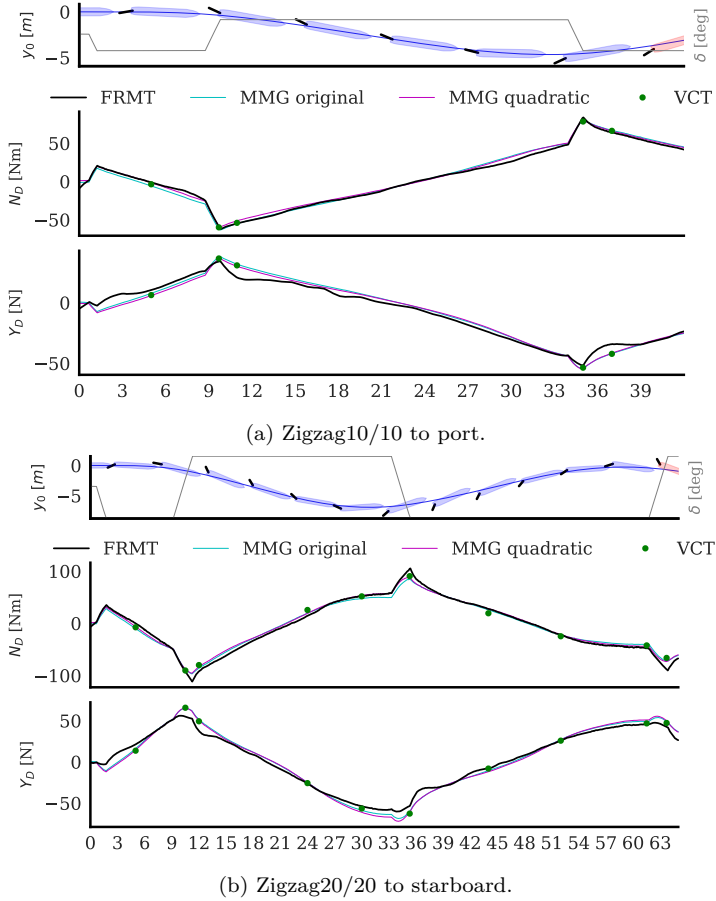
Figure 4.24: Inverse dynamics forces during the zigzag tests compared to predictions with the MMG models.

(a) Zigzag10/10 to port.

(b) Zigzag10/10 to starboard.

(c) Zigzag20/20 to port.

(d) Zigzag20/20 to starboard.
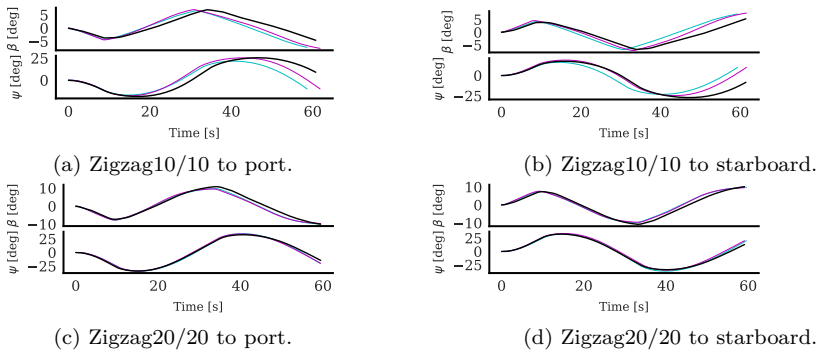
Figure 4.25: Comparison of zigzag tests between Optiwise experiments (black) and simulations with the MMG original (cyan) and MMG quadratic (purple).

53

Discussion

This thesis has demonstrated that identifying parametric manoeuvring models from standard manoeuvres is challenged by high multicollinearity among many model parameters. This issue is well-documented; Yoon and Rhee (2003) highlighted the difficulties in separately determining regression coefficients, and Wang and Zou (2018) discussed how multicollinearity can lead to parameter drift, resulting in unphysical models, as shown in this thesis.

Figure 5.1 presents a proposed flowchart for mitigating multicollinearity, addressing the challenges of correctly separating hull and rudder forces, as well as drift and yaw rate-dependent forces. It was shown in Paper 4 that a more accurate separation between hull and rudder forces can be achieved by introducing a deterministic semi-empirical rudder model, resulting in a more physically accurate model. Another effective approach is to measure the rudder forces, which yielded excellent results for the Optiwise test case in Paper 5.
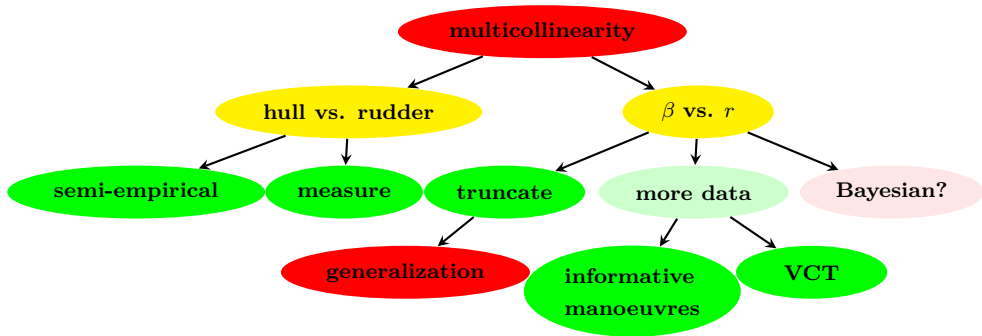
Figure 5.1: Flowchart for mitigating multicollinearity based on the research presented in this thesis.

Mitigating multicollinearity between drift and yaw rate-dependent parameters during standard manoeuvres is more challenging. Abkowitz (1980), Luo et al. (2016), Xu et al. (2019), Liu et al. (2024), and Paper 3 addressed this by truncating polynomials using various methods to select which parameters to remove. This approach is valid if the truncation method correctly identifies which parameters are identifiable from the data. However, model generalization inevitably suffers when parameters are removed, as certain regression terms may only become significant under specific conditions, such as sailing in wind. Truncated models may perform well when simulating conditions similar to the data, such as other standard manoeuvres, but excessive extrapolation should be avoided, as shown in Paper 4.

More informative data are needed to mitigate multicollinearity without reducing model generalization. Yoon and Rhee (2003) emphasized the importance of designing experiments that ensure persistence of excitation. They suggested using specific input

scenarios that maximize data information content, such as D-optimal designs. Wang et al. (2020) and Miller (2021) proposed using a pseudo-random sequence (PRS) for this purpose. These manoeuvres require more space than a model test basin provides, necessitating full-scale ship tests at sea or radio-controlled models on a lake.

Another option for gathering more informative data is conducting VCT calculations. Paper 5 demonstrated that a physically accurate model can be identified in this way, effectively overcoming the multicollinearity problem while maintaining good model generalization.

If a VCT is infeasible, prior knowledge of drift and yaw rate forces can be incorporated, akin to the semi-empirical rudder model. Chillcce and Moctar (2023) used a constrained least-squares algorithm, defining the sign and boundaries of the hydrodynamic derivatives based on prior knowledge from VCT. Taimuri et al. (2020) proposed calculating hydrodynamic derivatives from semi-empirical formulas combined with corrections from a reference ship. Bayesian modeling offers a more refined approach to expressing prior knowledge as prior probability densities. Xue et al. (2020) used a Bayesian approach for parameter identification in manoeuvring models, employing an optimizer to suggest priors. A more accurate, though demanding, method would be to specify priors based on the estimation of hydrodynamic derivatives from many ships, which could be an interesting topic for future work, as discussed in further detail in chapter 7.

Conclusions

This thesis investigated the enhancement of ship manoeuvring models through the integration of prior knowledge embedded in parametric model structures and semi-empirical formulas together with additional VCT calculations. The main findings and conclusions are presented below, as well as the impacts of the work.

A parametric model structure and parameter identification technique for roll motion

As demonstrated in Paper 1, inverse dynamics regression (referred to as the derivation approach in that paper) is an efficient method for identifying parameters in parametric roll motion models. The study also showed that 250 roll decay tests were well described by the quadratic model structure. Consequently, this model structure was proposed as a robust framework for system identification of roll motion, offering good generalization.

Parameter identification techniques for ship manoeuvring models

This thesis proposes parameter identification techniques for both FT and CT (VCT) data.

A new recursive inverse dynamics regression method for FT data, was proposed in Paper 3. This method combined inverse dynamics with an EKF in a two-step iterative approach (Yoon and Rhee 2003). The initial input model for this method was a linear maneuvering model with hydrodynamic derivatives estimated using semi-empirical formulas from the literature. The new method was found to be capable of effectively handling measurement noise and estimating the parameters within the models.

A method was also proposed for CT data, with its novelty lying in the inclusion of the most critical states during maneuvers into the design of the VCT matrix. This consequently ensured coverage of the relevant regions of the state space. The method successfully identified a model for the Optiwise test case that showed strong agreement with the measured rudder forces and inverse dynamics forces for the FRMTs. This model also demonstrated good consistency with the corresponding closed-loop simulations. These results indicate that a physically accurate model with high prediction accuracy can be obtained using this proposed method, given accurate VCT data.

Parametric model structure with good generalization identifiable from standard maneuvers

It was found in Paper 3 that a very complex manoeuvring model, such as the full Abkowitz model, could not be identified from standard manoeuvres where high multicollinearity was observed between the hydrodynamic derivatives. Model truncation was used to reduce the number of hydrodynamic derivatives to obtain more identifiable models while mitigating multicollinearity between the remaining hydrodynamic derivatives.

Model generalization from simpler to more complex maneuvers was assessed by identifying truncated models from zigzag tests to predict significantly different turning circle tests. The advance and tactical diameters were predicted within 5% error for the two investigated ships. It was concluded that a truncated Abkowitz model identified from standard maneuvers is capable of satisfactorily simulating other standard maneuvers.

However, Paper 4 showed that the truncated models in Paper 3 did not generalize well when the ship was exposed to external wind forces. The model was found to be physically incorrect, despite being mathematically correct. The identification method failed to correctly separate the hull and rudder forces when only the total force of the inverse dynamics was available. A deterministic semi-empirical rudder model was proposed as a replacement for the data-driven rudder model to address this shortcoming. This steered the identification toward a more physically correct model with lower multicollinearity and better generalization to wind conditions, proving to be an effective mitigation strategy.

Despite these improvements, issues with multicollinearity persisted due to the high correlation between yaw rate and drift during standard maneuvers, preventing the identification of perfectly physically correct models in Paper 4. It was demonstrated that these problems could be resolved through additional VCT calculations to obtain more informative data, which proved to be an effective approach to mitigating this aspect of the multicollinearity, particularly in cases where CFD calculations are a viable and accurate option.

Semi-empirical formulas to improve generalization

Several semi-empirical formulas available in the literature that incorporate prior hydrodynamic knowledge, potentially aiding model identification. Semi-empirical methods to predict roll damping were investigated in Paper 1. Predictions with Ikeda's method, including 2D potential flow strip calculations, were in fair agreement with roll decay tests for 15 investigated ships. A more in-depth analysis of roll damping was conducted for the KVLCC2 test case in Paper 2. In this study, the 2D potential flow strip calculation was replaced by a more modern potential flow code. This combined approach produced roll motion predictions with high accuracy. It was thereby concluded that Ikeda's method provides a good semi-empirical method for predicting viscous roll damping.

Prior knowledge from semi-empirical formulas in the literature was used to estimate the initial input model for the recursive inverse dynamics regression method. This provided a reasonable prediction model of the EKF in the first iteration of this two-step method.

In Paper 4, a new semi-empirical rudder model was proposed for the twin rudder wPCC test case based on various semi-empirical formulas from the literature. The model was in good agreement with the VCT data in Paper 4 and 5. A modified quadratic version of the MMG semi-empirical rudder model was proposed in Paper 5. It was shown that this model could satisfactorily predict the VCT data and the measured rudder forces during zigzag model tests for the single rudder Optiwise test case. The semi-empirical rudder model from Paper 4 and the modified quadratic MMG rudder model from Paper 5 belong to the same family of semi-empirical lifting-line rudder models, shown to be suitable for describing the true forces related to the rudder/rudders during standard manoeuvres.

These examples have demonstrated that incorporating prior knowledge of ship hydrodynamics by using existing semi-empirical formulas from the literature can enhance the identification of ship dynamics models. This approach is particularly beneficial for data with insufficient persistence of excitation, leading to more physically accurate models with improved generalization.

Impact of this work

Throughout this research, inverse dynamics has proven to be a valuable tool for analyzing the forces acting on a ship during an FT. Comparing inverse dynamics forces with model force predictions provides a more informative assessment of model performance than through open-loop or closed-loop simulations. This approach ensures that the model and the experiment are always in the same state, which is not the case for simulations. From an engineering perspective, recalculating FT accelerations as forces is more convenient, especially when comparing them with forces from static VCT. Additionally, preprocessing FT data using inverse dynamics enables parameter identification in a manner similar to that of CT data.

This thesis has demonstrated that identifying a physically correct model with excellent generalization solely from standard manoeuvres FT data is challenging. The identification process may yield models that are mathematically correct but physically incorrect. These models may still predict other standard manoeuvres within a reasonable level of extrapolation. However, it has been shown that these models do not generalize well when wind forces are introduced.

Incorporating additional data from well-known semi-empirical models and VCT calculations improves the physical correctness and generalization of these models for applications requiring large extrapolations, such as those involving wind conditions.

Chapter 7

Future work

The rigid body assumption during maneuvers is reasonable considering the relatively low accelerations and bending of the hull girder during maneuvers, at least in the absence of waves. However, there are other assumptions and limitations that can be addressed through future research, as described below.

Only data from standard test types, such as turning circles or zigzag tests were used in this thesis, since they are commonly available for ships

It has been shown in this thesis that identifying a physically correct manoeuvring model from data with only standard maneuvers is very difficult, due to high multicollinearity and insufficient persistence of excitation. It was further demonstrated that prior knowledge of manoeuvring hydrodynamics embedded in the model structure together with good semi-empirical formulas can help to mitigate, but not completely resolve, these problems. More informative data are needed to identify a fully physically correct model that could be obtained with other types of maneuvers, such as pseudo random binary sequence (PRBS) (Yoon and Rhee 2003; Wang et al. 2020). Studies of system identification based on these kinds of informative maneuvers have primarily been conducted with simulated data. Collecting experimental data for these informative maneuvers would be a significant contribution, since they require more space than is available in a model test basin. Miller (2021) conducted such tests on a lake and noted the difficulty and time-consuming nature of this approach. More work is needed to establish reliable experimental research data from maneuvers in which all modes of the manoeuvring dynamics of the ship are excited, which could perhaps be conducted with one of the more well-researched test cases, such as KVLCC2.

Bayesian modeling

In contrast to the methods used in this thesis, which incorporate prior knowledge of ship hydrodynamics, Bayesian modeling offers a more sophisticated approach by expressing prior knowledge as prior probability densities. Informative priors can guide parameter identification toward hydrodynamic derivatives that are physically reasonable, based on prior knowledge from similar ships, even for standard manoeuvres that lack persistence of excitation. However, developing informative priors for hydrodynamic derivatives would require significant research effort, such as creating a comprehensive database of identified manoeuvring models for numerous ships. This effort would enable the identification of models with much better generalization from standard manoeuvres. Additionally, Bayesian modeling with informative hydrodynamic priors could have valuable applications in the system identification of full-scale ship operations and autonomous ships.

Calm water assumption

The sea is never calm, so this assumption within manoeuvring greatly simplifies the real-world conditions encountered by ships. Relaxing this assumption would significantly complicate system identification. The fluid-memory effect would need to be addressed, and the assumption of constant added mass would no longer be valid. An alternative approach to those presented in this thesis would be required. A data-driven model for viscous manoeuvring forces could potentially be coupled with potential flow calculations, akin to the method used for roll motion in Paper 2.

The free surface effects and the influence of the roll were not included in the VCT data

It was shown in Paper 5 that a manoeuvring model could be identified from VCT to predict standard maneuvers with good precision for only one of the test cases. It was argued that this discrepancy was due to the unjustified assumption of neglecting the free surface and roll influence for this ship. This statement should be validated through further investigation. In addition, a better understanding of when these assumptions can be applied is necessary.

References

Abkowitz, M. A. (1964). "Ship hydrodynamics - steering and manoeuvrability". en. In: *Hydro- and Aerodynamics Laboratory, Hydrodynamics Section, Lyngby, Denmark, Report No. Hy-5, Lectures.*

Abkowitz, M. A. (1980). "MEASUREMENT OF HYDRODYNAMIC CHARACTERISTICS FROM SHIP MANEUVERING TRIALS BY SYSTEM IDENTIFICATION". In: Number: No. 10.

Ahnert, K. and Abel, M. (2007). "Numerical differentiation of experimental data: local versus global methods". In: *Computer Physics Communications* 177.10, pp. 764–774. ISSN: 0010-4655. DOI: 10.1016/j.cpc.2007.03.009.

Alexandersson, M. (2022). *wPCC manoeuvring model tests.* en. Publisher: Mendeley Data. DOI: 10.17632/j5zdrhr9bf.2.

Alexandersson, M. (2024). "wPCC manoeuvring model tests". en. In: 4. Publisher: Mendeley Data. DOI: 10.17632/j5zdrhr9bf.4.

Alexandersson, M. and Kjellberg, M. (2021). *KVLCC2 roll decay.* en. Publisher: Mendeley. DOI: 10.17632/2stvkyngj9.1.

Alexandersson, M., Kjellberg, M., Mao, W., and Ringsberg, J. W. (2021a). "Prediction of roll motion using fully nonlinear potential flow and Ikeda's method". In: *Proceedings of the Thirty-first (2021) International Ocean and Polar Engineering Conference.* Rhodes, Greece: International Society of Offshore and Polar Engineers (ISOPE). ISBN: 978-1-880653-82-1.

Alexandersson, M., Mao, W., and Ringsberg, J. W. (2021b). "Analysis of roll damping model scale data". In: *Ships and Offshore Structures* 16.sup1. Publisher: Taylor & Francis _eprint: https://www.tandfonline.com/doi/pdf/10.1080/17445302.2021.1907070, pp. 85–92. ISSN: 1744-5302. DOI: 10.1080/17445302.2021.1907070.

Alexandersson, M., Mao, W., and Ringsberg, J. W. (2022). "System identification of Vessel Manoeuvring Models". In: *Ocean Engineering* 266, p. 112940. ISSN: 0029-8018. DOI: 10.1016/j.oceaneng.2022.112940.

Alexandersson, M., Mao, W., Ringsberg, J. W., and Kjellberg, M. (2024). "System identification of a physics-informed ship model for better predictions in wind conditions". In: *Ocean Engineering* 310, p. 118613. ISSN: 0029-8018. DOI: 10.1016/j.oceaneng.2024.118613.

Araki, M., Sadat-Hosseini, H., Sanada, Y., Tanimoto, K., Umeda, N., and Stern, F. (2012). "Estimating maneuvering coefficients using system identification methods with experimental, system-based, and CFD free-running trial data". en. In: *Ocean Engineering* 51. 99 citations (Crossref/DOI) [2025-01-05], pp. 63–84. ISSN: 0029-8018. DOI: 10.1016/j.oceaneng.2012.05.001.

Åström, K. J. and Källström, C. G. (1976). "Identification of ship steering dynamics". en. In: *Automatica* 12.1, pp. 9–22. ISSN: 0005-1098. DOI: 10.1016/0005-1098(76)90064-9.

Brix, J. E. (1993). *Manoeuvring Technical Manual. ISBN: 978-3-87743-902-9.* en. Google-Books-ID: CMJ1NAAACAAJ. Seehafen-Verlag. ISBN: 978-3-87743-902-9.

Brown, R. G. and Hwang, P. Y. C. (1997). *Introduction to random signals and applied kalman filtering : with MATLAB exercises and solutions.* Wiley. ISBN: 978-0-471-12839-7.

Brunton, S. L., Proctor, J. L., and Kutz, J. N. (2016). "Discovering governing equations from data by sparse identification of nonlinear dynamical systems". en. In: *Proceedings of the National Academy of Sciences* 113.15, pp. 3932–3937. ISSN: 0027-8424, 1091-6490. DOI: 10.1073/pnas.1517384113.

Casado, M. H. and Ferreiro, R. (2005). "Identification of the nonlinear ship model parameters based on the turning test trial and the backstepping procedure". en. In: *Ocean Engineering* 32.11, pp. 1350–1369. ISSN: 0029-8018. DOI: 10.1016/j.oceaneng.2004.11.003.

Chen, L., Yang, P., Li, S., Liu, K., Wang, K., and Zhou, X. (2023). "Online modeling and prediction of maritime autonomous surface ship maneuvering motion under ocean waves". In: *Ocean Engineering* 276, p. 114183. ISSN: 0029-8018. DOI: 10.1016/j.oceaneng.2023.114183.

Chillcce, G. and Moctar, O. el (2023). "Data-driven system identification of hydrodynamic maneuvering coefficients from free-running tests". In: *Physics of Fluids* 35.5, p. 057122. ISSN: 1070-6631. DOI: 10.1063/5.0148219.

Costa, A. C., Xu, H., and Guedes Soares, C. (2021). "Robust Parameter Estimation of an Empirical Manoeuvring Model Using Free-Running Model Tests". en. In: *Journal of Marine Science and Engineering* 9.11. Number: 11 Publisher: Multidisciplinary Digital Publishing Institute, p. 1302. ISSN: 2077-1312. DOI: 10.3390/jmse9111302.

Dong, Q., Wang, N., Song, J., Hao, L., Liu, S., Han, B., and Qu, K. (2023). "Math-data integrated prediction model for ship maneuvering motion". In: *Ocean Engineering* 285, p. 115255. ISSN: 0029-8018. DOI: 10.1016/j.oceaneng.2023.115255.

Faber, H., Soest, A. J. v., and Kistemaker, D. A. (2018). "Inverse dynamics of mechanical multibody systems: An improved algorithm that ensures consistency between kinematics and external forces". en. In: *PLOS ONE* 13.9. Publisher: Public Library of Science, e0204575. ISSN: 1932-6203. DOI: 10.1371/journal.pone.0204575.

Fossen, T. I. (2011). *Handbook of Marine Craft Hydrodynamics and Motion Control*. en. John Wiley & Sons.

France, W. N., Levadou, M., Treakle, T. W., Paulling, J. R., Michel, R. K., and Moore, C. (2001). "An Investigation of Head-Sea Parametric Rolling and its Influence on Container Lashing Systems". en. In: *SNAME Annual Meeting 2001 Presentation*, p. 24.

Hajivand, A. and Mousavizadegan, S. H. (2015). "Virtual simulation of maneuvering captive tests for a surface vessel". In: *International Journal of Naval Architecture and Ocean Engineering* 7.5. 29 citations (Crossref/DOI) [2025-01-05], pp. 848–872. ISSN: 2092-6782. DOI: 10.1515/ijnaoe-2015-0060.

Haninger, K. and Tomizuka, M. (2019). *Nonparametric Inverse Dynamic Models for Multimodal Interactive Robots*. arXiv:1901.03872 [cs]. DOI: 10.48550/arXiv.1901.03872.

He, H.-W., Wang, Z.-H., Zou, Z.-J., and Liu, Y. (2022). "Nonparametric modeling of ship maneuvering motion based on self-designed fully connected neural network". en. In: *Ocean Engineering* 251, p. 111113. ISSN: 00298018. DOI: 10.1016/j.oceaneng.2022.111113.

He, H.-W. and Zou, Z.-J. (2020). "Black-Box Modeling of Ship Maneuvering Motion Using System Identification Method Based on BP Neural Network". en. In: *Volume 6B: Ocean Engineering.* Virtual, Online: American Society of Mechanical Engineers, V06BT06A037. ISBN: 978-0-7918-8438-6. DOI: `10.1115/OMAE2020-18069`.

Himeno, Y. (1981). "Prediction of ship roll damping - state of the art." In: *University of Michigan Department of Naval Architecture and Marine Engineering, (Report)* 239.

Hughes, M. J., Campbell, B. L., Belknap, W. F., and Smith, T. C. (2011). *TEMPEST Level-0 Theory:* en. Tech. rep. Fort Belvoir, VA: Defense Technical Information Center. DOI: `10.21236/ADA553545`.

Ikeda, Y. (1978). "On eddy making component of roll damping force on naked hull". en. In: *University of Osaka Prefacture, Department of Naval Architecture, Japan, Report No. 00403, Published in: Journal of Society of Naval Architects of Japan, Volume 142.*

Ikeda, Y., Himeno, Y., and Tanaka, N. (1978). "Components of Roll Damping of Ship at Forward Speed". en. In: *Journal of the Society of Naval Architects of Japan* 1978.143, pp. 113–125. ISSN: 0514-8499, 1884-2070. DOI: `10.2534/jjasnaoe1968.1978.113`.

IMO (2002). *Standards for ship manoeuvrability, Resolution MSC 137(76).*

IMO (2006). *1200 - Interim Guidelines For Alternative Assessment Of The Weather Criterion - Netherlands Regulatory Framework (NeRF) – Maritime.*

Inoue, S., Hirano, M., Kijima, K., and Takashina, J. (1981). "A practical calculation method of ship maneuvering motion". en. In: *International Shipbuilding Progress* 28.325. Publisher: SAGE Publications, pp. 207–222. ISSN: 0020-868X. DOI: `10.3233/ISP-1981-2832502`.

ITTC (2008). *The Maneuvering Committee of ITTC, Final report and recommendations to the 25th ITTC, in Proceedings of the 25th International Towing Tank Conference.*

Kawahara, Y., Maekawa, K., and Ikeda, Y. (2011). "A Simple Prediction Formula of Roll Damping of Conventional Cargo Ships on the Basis of Ikeda's Method and Its Limitation". en. In: *Contemporary Ideas on Ship Stability and Capsizing in Waves.* Ed. by M. Almeida Santos Neves, V. L. Belenky, J. O. de Kat, K. Spyrou, and N. Umeda. Fluid Mechanics and Its Applications. Dordrecht: Springer Netherlands, pp. 465–486. ISBN: 978-94-007-1482-3. DOI: `10.1007/978-94-007-1482-3_26`.

Kjellberg, M. (2013). "Fully Nonlinear Unsteady Three-Dimensional Boundary Element Method for Ship Motions in Waves". en. ISBN: 9789173858700. PhD thesis. Chalmers University of Technology.

Kjellberg, M., Gerhardt, F., and Werner, S. (2023). "Sailing Performance of Wind-Powered Cargo Vessel in Unsteady Conditions". In: *Journal of Sailing Technology* 8.01, pp. 218–254. ISSN: 2475-370X. DOI: `10.5957/jst/2023.8.12.218`.

Kurtz, V., Castro, A., Önol, A. Ö., and Lin, H. (2023). *Inverse Dynamics Trajectory Optimization for Contact-Implicit Model Predictive Control.* arXiv:2309.01813 [cs]. DOI: `10.48550/arXiv.2309.01813`.

Lewis, E. V. (1989). *Principles of Naval Architecture Second Revision: Volume III—Motions in Waves and Contrallability.* en. The Society of Naval Architects and Marine Engineers.

Liu, A., Xue, Y., Qin, H., and Zhu, Z. (2024). "Physics-informed identification of marine vehicle dynamics using hydrodynamic dictionary library-inspired adaptive regression". In: *Ocean Engineering* 296, p. 117013. ISSN: 0029-8018. DOI: `10.1016/j.oceaneng.2024.117013`.

Liu, Y., Zou, L., Zou, Z., and Guoa, H. (2018). "Predictions of ship maneuverability based on virtual captive model tests". English. In: *Engineering Applications of Computational Fluid Mechanics* 12.1. 9 citations (Crossref/DOI) [2025-01-05] 9 citations (Crossref/DOI) [2025-01-05] 9 citations (Crossref/DOI) [2025-01-05], pp. 334–353. ISSN: 1994-2060. DOI: `10.1080/19942060.2018.1439773`.

Ljung, L. (2010). "Perspectives on system identification". In: *Annual Reviews in Control* 34.1, pp. 1–12. ISSN: 1367-5788. DOI: `10.1016/j.arcontrol.2009.12.001`.

Ljung, L., Glad, T., and Hansson, A. (2021). *Modeling and Identification of Dynamic Systems.* en. Google-Books-ID: Q3GhzgEACAAJ. Studentlitteratur AB. ISBN: 978-91-44-15345-2.

Luo, W., Guedes Soares, C., and Zou, Z. (2016). "Parameter Identification of Ship Maneuvering Model Based on Support Vector Machines and Particle Swarm Optimization". en. In: *Journal of Offshore Mechanics and Arctic Engineering* 138.3, p. 031101. ISSN: 0892-7219, 1528-896X. DOI: `10.1115/1.4032892`.

Mastalli, C., Chhatoi, S. P., Corbères, T., Tonneau, S., and Vijayakumar, S. (2023). *Inverse-Dynamics MPC via Nullspace Resolution.* arXiv:2209.05375 [cs, eess]. DOI: `10.48550/arXiv.2209.05375`.

Matusiak, J. (2021). *Dynamics of a Rigid Ship - with applications, 3rd edition.* ISBN: 978-952-64-0398-4.

Miller, A. (2021). "Ship Model Identification with Genetic Algorithm Tuning". en. In: *Applied Sciences* 11.12, p. 5504. ISSN: 2076-3417. DOI: `10.3390/app11125504`.

Moctar, O. el, Lantermann, U., and Chillcce, G. (2022). "An efficient and accurate approach for zero-frequency added mass for maneuvering simulations in deep and shallow water". In: *Applied Ocean Research* 126, p. 103259. ISSN: 0141-1187. DOI: `10.1016/j.apor.2022.103259`.

Moctar, O. el, Lantermann, U., Mucha, P., Höpken, J., and Schellin, T. E. (2014). "RANS-Based Simulated Ship Maneuvering Accounting for Hull-Propulsor-Engine Interaction". In: *Ship Technology Research* 61.3. 18 citations (Crossref/DOI) [2025-01-05] Publisher: Taylor & Francis _eprint: https://doi.org/10.1179/str.2014.61.3.003, pp. 142–161. ISSN: 0937-7255. DOI: `10.1179/str.2014.61.3.003`.

Nielsen, R. E., Papageorgiou, D., Nalpantidis, L., Jensen, B. T., and Blanke, M. (2022). "Machine learning enhancement of manoeuvring prediction for ship Digital Twin using full-scale recordings". en. In: *Ocean Engineering* 257, p. 111579. ISSN: 00298018. DOI: `10.1016/j.oceaneng.2022.111579`.

Nomoto, K., Taguchi, T., Honda, K., and Hirano, S. (1957). "On the steering qualities of ships". en. In: *Osaka University, Department of Naval Architecture, Japan,*

Published in: International Shipbuilding Progress, ISP, Volume 4, No. 35, 1957 pp. 354-370.

Norrbin, N. H. (1971). "Theory and observations on the use of a mathematical model for ship manoeuvring in deep and confined waters". en. In: *Publication 68 of the Swedish State Shipbuilding Experimental Tank, Göteborg, Sweden, Proceedings of the 8th Symposium on Naval Hydrodynamics, ONR, Pasadena, California, pp. 807-905.*

Ogawa, A. and Kasai, H. (1978). "On the mathematical model of manoeuvring motion of ships". en. In: *International Shipbuilding Progress* 25.292. Publisher: SAGE Publications, pp. 306–319. ISSN: 0020-868X. DOI: 10.3233/ISP-1978-2529202.

Perera, L. P., Oliveira, P., and Guedes Soares, C. (2015). "System Identification of Nonlinear Vessel Steering". en. In: *Journal of Offshore Mechanics and Arctic Engineering* 137.3, p. 031302. ISSN: 0892-7219, 1528-896X. DOI: 10.1115/1.4029826.

Piehl, H. P. (2016). "Ship Roll Damping Analysis". Doctoral thesis. Germany: University of Duisburg-Essen.

Rajesh, G. and Bhattacharyya, S. K. (2008). "System identification for nonlinear maneuvering of large tankers using artificial neural network". en. In: *Applied Ocean Research* 30.4, pp. 256–263. ISSN: 0141-1187. DOI: 10.1016/j.apor.2008.10.003.

Rauch, H. E., Striebel, C. T., and Tung, F. (1965). "Maximum likelihood estimates of linear dynamic systems". In: *AIAA Journal* 3. ADS Bibcode: 1965AIAAJ...3.1445R, pp. 1445–1450. ISSN: 0001-1452. DOI: 10.2514/3.3166.

Revestido Herrero, E. and Velasco González, F. J. (2012). "Two-step identification of non-linear manoeuvring models of marine vessels". en. In: *Ocean Engineering* 53, pp. 72–82. ISSN: 0029-8018. DOI: 10.1016/j.oceaneng.2012.07.010.

RoyChoudhury, S., Dash, A. K., Nagarajan, V., and Sha, O. P. (2017). "CFD simulations of steady drift and yaw motions in deep and shallow water". In: *Ocean Engineering* 142, pp. 161–184. ISSN: 0029-8018. DOI: 10.1016/j.oceaneng.2017.06.058.

Sakamoto, N., Carrica, P. M., and Stern, F. (2012). "URANS simulations of static and dynamic maneuvering for surface combatant: part 1. Verification and validation for forces, moment, and hydrodynamic derivatives". en. In: *Journal of Marine Science and Technology* 17.4, pp. 422–445. ISSN: 1437-8213. DOI: 10.1007/s00773-012-0178-x.

Sakamoto, N., Kobayashi, H., and Ohashi, K. (2021). *CFD Based Turning Circle Maneuvering Simulation for a Merchant Ship with High-lift Rudder.*

"Holdout Evaluation" (2017). en. In: *Encyclopedia of Machine Learning and Data Mining.* Ed. by C. Sammut and G. I. Webb. Boston, MA: Springer US, pp. 624–624. ISBN: 978-1-4899-7687-1. DOI: 10.1007/978-1-4899-7687-1_369.

Shi, C., Zhao, D., Peng, J., and Shen, C. (2009). "Identification of Ship Maneuvering Model Using Extended Kalman Filters". en. In: *International Journal on Marine Navigation and Safety of Sea Transportation* 3.1, p. 6.

SIMMAN (2014). "Workshop on verification and validation of ship manoeuvring simulation methods". In: Copenhagen, Denmark.

Simonsen, C. D. (2014). "KCS PMM tests with appended hull". In: *Proceedings of Workshop on Verification and Validation of Ship Manoeuvring Simulation Methods.* Copenhagen, Denmark.

Söder, C.-J., Rosén, A., Werner, S., Huss, M., and Kuttenkeuler, J. (2019). "Assessment of Ship Roll Damping Through Full Scale and Model Scale Experiments and Semi-empirical Methods". en. In: *Contemporary Ideas on Ship Stability: Risk of Capsizing*. Ed. by V. L. Belenky, K. J. Spyrou, F. van Walree, M. Almeida Santos Neves, and N. Umeda. Fluid Mechanics and Its Applications. Cham: Springer International Publishing, pp. 177–190. ISBN: 978-3-030-00516-0. DOI: `10.1007/978-3-030-00516-0_10`.

Stern, F., Agdraup, K., Kim, S. Y., Hochbaum, A. C., Rhee, K. P., Quadvlieg, F., Perdon, P., Hino, T., Broglia, R., and Gorski, J. (2011). "Experience from SIMMAN 2008—The First Workshop on Verification and Validation of Ship Maneuvering Simulation Methods". en. In: *Journal of Ship Research* 55.02, pp. 135–147. ISSN: 0022-4502, 1542-0604. DOI: `10.5957/jsr.2011.55.2.135`.

Sun, G. and Ding, Y. (2023). "High-order inverse dynamics of serial robots based on projective geometric algebra". en. In: *Multibody System Dynamics* 59.3, pp. 337–362. ISSN: 1573-272X. DOI: `10.1007/s11044-023-09915-7`.

Sutulo, S. and Guedes Soares, C. (2014). "An algorithm for offline identification of ship manoeuvring mathematical models from free-running tests". en. In: *Ocean Engineering* 79, pp. 10–25. ISSN: 0029-8018. DOI: `10.1016/j.oceaneng.2014.01.007`.

Sutulo, S. and Soares, C. G. (2004). "Synthesis of experimental designs of maneuvering captive-model tests with a large number of factors". en. In: *Journal of Marine Science and Technology* 9.1. 10 citations (Crossref/DOI) [2025-01-05], pp. 32–42. ISSN: 1437-8213. DOI: `10.1007/s00773-003-0169-z`.

Taimuri, G., Matusiak, J., Mikkola, T., Kujala, P., and Hirdaris, S. (2020). "A 6-DoF maneuvering model for the rapid estimation of hydrodynamic actions in deep and shallow waters". en. In: *Ocean Engineering* 218. 50 citations (Crossref/DOI) [2025-01-05], p. 108103. ISSN: 00298018. DOI: `10.1016/j.oceaneng.2020.108103`.

Tiano, A. and Blanke, M. (1997). "Multivariable identification of ship steering and roll motions". en. In: *Transactions of the Institute of Measurement and Control* 19.2, pp. 63–77. ISSN: 0142-3312, 1477-0369. DOI: `10.1177/014233129701900202`.

Tzeng, C.-Y. and Chen, J.-F. (1999). "FUNDAMENTAL PROPERTIES OF LINEAR SHIP STEERING DYNAMIC MODELS". en. In: *Journal of Marine Science and Technology* 7.2, p. 10.

Villa, D., Franceschi, A., and Viviani, M. (2020). "Numerical Analysis of the Rudder–Propeller Interaction". en. In: *Journal of Marine Science and Engineering* 8.12. Number: 12 Publisher: Multidisciplinary Digital Publishing Institute, p. 990. ISSN: 2077-1312. DOI: `10.3390/jmse8120990`.

Wang, T., Li, G., Hatledal, L. I., Skulstad, R., Aesoy, V., and Zhang, H. (2021). "Incorporating Approximate Dynamics Into Data-Driven Calibrator: A Representative Model for Ship Maneuvering Prediction". en. In: *IEEE Transactions on Industrial Informatics*, pp. 1–1. ISSN: 1551-3203, 1941-0050. DOI: `10.1109/TII.2021.3088404`.

Wang, Z., Guedes Soares, C., and Zou, Z. (2020). "Optimal design of excitation signal for identification of nonlinear ship manoeuvring model". In: *Ocean Engineering* 196, p. 106778. ISSN: 0029-8018. DOI: `10.1016/j.oceaneng.2019.106778`.

Wang, Z. and Zou, Z. (2018). *Quantifying Multicollinearity in Ship Manoeuvring Modeling by Variance Inflation Factor*. Madrid: ASME 2018 37th International Conference on Ocean, Offshore and Arctic. DOI: `10.1115/OMAE2018-77121`.

Whicker, L. F. and Fehlner, L. F. (1958). *Free-Stream Characteristics of A Family of Low-Aspect-Ratio, All-Movable Control Surfaces for Application to Ship Design:* en. Tech. rep. Fort Belvoir, VA: Defense Technical Information Center. DOI: `10.21236/ADA014272`.

Xu, H., Hassani, V., and Guedes Soares, C. (2019). "Uncertainty analysis of the hydrodynamic coefficients estimation of a nonlinear manoeuvring model based on planar motion mechanism tests". In: *Ocean Engineering* 173, pp. 450–459. ISSN: 0029-8018. DOI: `10.1016/j.oceaneng.2018.12.075`.

Xue, Y., Chen, G., Li, Z., Xue, G., Wang, W., and Liu, Y. (2022). "Online identification of a ship maneuvering model using a fast noisy input Gaussian process". English. In: *Ocean Engineering* 250. ISSN: 0029-8018. DOI: `10.1016/j.oceaneng.2022.110704`.

Xue, Y., Liu, Y., Ji, C., and Xue, G. (2020). "Hydrodynamic parameter identification for ship manoeuvring mathematical models using a Bayesian approach". en. In: *Ocean Engineering* 195, p. 106612. ISSN: 0029-8018. DOI: `10.1016/j.oceaneng.2019.106612`.

Xue, Y., Liu, Y., Xue, G., and Chen, G. (2021). "Identification and Prediction of Ship Maneuvering Motion Based on a Gaussian Process with Uncertainty Propagation". en. In: *Journal of Marine Science and Engineering* 9.8, p. 804. ISSN: 2077-1312. DOI: `10.3390/jmse9080804`.

Yasukawa, H. and Yoshimura, Y. (2015). "Introduction of MMG standard method for ship maneuvering predictions". en. In: *Journal of Marine Science and Technology* 20.1, pp. 37–52. ISSN: 1437-8213. DOI: `10.1007/s00773-014-0293-y`.

Yoon, H. K. and Rhee, K. P. (2003). "Identification of hydrodynamic coefficients in ship maneuvering equations of motion by Estimation-Before-Modeling technique". In: *Ocean Engineering* 30.18, pp. 2379–2404. ISSN: 0029-8018. DOI: `10.1016/S0029-8018(03)00106-9`.

Yoon, H., Simonsen, C. D., Benedetti, L., Longo, J., Toda, Y., and Stern, F. (2015). "Benchmark CFD validation data for surface combatant 5415 in PMM maneuvers – Part I: Force/moment/motion measurements". In: *Ocean Engineering* 109, pp. 705–734. ISSN: 0029-8018. DOI: `10.1016/j.oceaneng.2015.04.087`.

Zhang, Z. and Ren, J. (2021). "Locally Weighted Non-Parametric Modeling of Ship Maneuvering Motion Based on Sparse Gaussian Process". en. In: *Journal of Marine Science and Engineering* 9.6. Number: 6 Publisher: Multidisciplinary Digital Publishing Institute, p. 606. ISSN: 2077-1312. DOI: `10.3390/jmse9060606`.

Zihao Wang, Wang, Z., Haitong Xu, Xu, H., Xia Li, Li Xia, Xia, L., Zao-Jian Zou, Zou, Z.-J., C. Guedes Soares, and Soares, C. G. (2020). "Kernel-based support vector regression for nonparametric modeling of ship maneuvering motion". In: *Ocean Engineering* 216. MAG ID: 3087411932, p. 107994. DOI: `10.1016/j.oceaneng.2020.107994`.

Analysis of roll damping model scale data

M. Alexandersson, W. Mao, and J. W. Ringsberg (2021b). "Analysis of roll damping model scale data". In: *Ships and Offshore Structures* 16.sup1. Publisher: Taylor & Francis _eprint: https://www.tandfonline.com/doi/pdf/10.1080/17445302.2021.1907070 pp. 85–92. ISSN: 1744-5302. DOI: 10.1080/17445302.2021.1907070

Prediction of roll motion using fully nonlinear potential flow and Ikeda's method

M. Alexandersson, M. Kjellberg, W. Mao, and J. W. Ringsberg (2021a). "Prediction of roll motion using fully nonlinear potential flow and Ikeda's method". In: *Proceedings of the Thirty-first (2021) International Ocean and Polar Engineering Conference.* Rhodes, Greece: International Society of Offshore and Polar Engineers (ISOPE). ISBN: 978-1-880653-82-1

Paper **3**

System identification of vessel manoeuvring models

System identification of a physics-informed ship model for better predictions in wind conditions

Identification of manoeuvring models for wind-assisted ships with large rudders using virtual captive tests

Alexandersson, M., Mao, W., Ringsberg, J. W., and Kjellberg, M. (2025). "Identification of manoeuvring models for wind-assisted ships with large rudders using virtual captive tests". Manuscript submitted to: *International Journal of Naval Architecture and Ocean Engineering.*